Title: Independent and distinct patterns of abnormal lateral orbitofrontal cortex activity during compulsive grooming and reversal learning normalize after fluoxetine

Authors
Elizabeth E Manning[1, *], Matthew A Geramita[2, *], Sean C Piantadosi[3, *], Susanne E Ahmari[2]

Affiliations:
1. School of Biological Sciences and Pharmacy; University of Newcastle; Newcastle, Australia
2. Translational Neuroscience Program, Department of Psychiatry, University of Pittsburgh, Pittsburgh, USA
3. Center for Neurobiology of Addiction, Pain, and Emotion, University of Washington, Seattle, USA

* These authors contributed equally

Corresponding Author:
Susanne E Ahmari
450 Technology Drive
Pittsburgh, PA 15219
412-624-3183
susanneahmari@gmail.com

Running title: LOFC activity during compulsions and reversal learning

Keywords: Orbitofrontal cortex, compulsion, reversal learning, calcium imaging, obsessive-compulsive disorder, Sapap3

Abstract word count: 237 (250)
Main text: 3916 (4000)
Figures: 8
Supplemental Figures: 8
Tables: 2

Abstract

Background: Patients with obsessive-compulsive disorder (OCD) display disrupted performance and abnormal lateral orbitofrontal cortex (LOFC) activity during reversal learning tasks, yet it is unknown whether compulsions and reversal learning deficits share a common neural substrate. To answer this question, we measured neural activity with *in vivo* calcium imaging in LOFC during compulsive grooming and reversal learning before and after fluoxetine treatment.

Methods: *Sapap3*-knockout (KO) mice were used as a model for OCD-relevant behaviors. *Sapap3*-KOs and control littermates were injected with virus encoding GCaMP6f and implanted with gradient-index lenses to visualize LOFC activity using miniature microscopes. Grooming, reversal learning, and neural activity were measured pre- and post-fluoxetine treatment (18mg/kg, 4 weeks).

Results: Baseline compulsive grooming and reversal learning impairments in KOs improve after fluoxetine treatment. Additionally, KOs display distinct patterns of abnormal LOFC activity during grooming and reversal learning, both of which normalize after fluoxetine. Finally, encoding of reversal learning and compulsive behavior are independent, as reversal learning-associated neurons are distributed randomly amongst grooming-associated neurons (i.e. overlap is what would be expected by chance).

Conclusions: In OCD, the LOFC is disrupted during both compulsive behaviors and reversal learning, yet whether these behaviors share common neural underpinnings is unknown. We find that the LOFC plays distinct and independent roles in compulsive grooming and impaired reversal learning and their improvement with fluoxetine. These findings suggest that LOFC plays separate roles in pathophysiology and treatment of different perseverative behaviors in OCD.

Introduction

Determining how disrupted neural activity gives rise to compulsive behaviors is vital for understanding obsessive compulsive disorder (OCD). It is commonly thought that compulsive behaviors and cognitive rigidity may share a pathologic neural substrate due to an association between compulsive behavior and abnormal performance (*1, 2*) and reaction times (*3-5*) during reversal learning tasks in OCD [though see (*6-8*)]. Additionally, patients with OCD show abnormal activity during reversal learning (*2, 3, 9, 10*) in the same orbitofrontal-striatal circuits that show abnormal activity during symptom provocation (*11-13*). However, it is currently unknown whether impaired reversal learning and compulsive behaviors stem from the same underlying abnormalities in orbitofrontal cortex (OFC) activity.

Determining whether the same OFC neurons show disrupted coding of both behaviors is one strategy to establish whether abnormal reversal learning and compulsive behaviors share common neural underpinnings. Since human neuroimaging technology lacks the single cell resolution necessary to test this idea, preclinical models are needed to define the precise pattern and overlap of neural activity between these distinct phenotypes. Features of the *Sapap3* knockout (KO) mouse model for OCD-relevant behaviors make it an ideal system to test this hypothesis (*14-16*). *Sapap3*, a post-synaptic density protein, is critical for cortico-striatal communication (*14, 17, 18*), and the *SAPAP3* gene family has been linked to OCD in candidate gene studies and in secondary analyses of genome wide association studies despite not meeting genome-wide level of significance (*19-22*). *SAPAP3* transcript levels in the OFC, caudate, and nucleus accumbens are lower in patients with OCD than unaffected comparison subjects (*23*). Additionally, *Sapap3*-KO mice display compulsive grooming which decreases following optogenetic activation of the lateral OFC [LOFC; (*15*)] or treatment with a first-line pharmacotherapy for OCD, the selective serotonin reuptake inhibitor (SSRI) fluoxetine (*14-16*). Finally, *Sapap3*-KO mice display impaired reversal learning (*24-27*), strengthening their relevance to OCD.

Here, using *in vivo* microendoscopic calcium imaging in freely-moving mice, we record activity of individual LOFC neurons in *Sapap3*-KOs and wild-type (WT) littermates during grooming and reversal learning before and after 4-weeks of fluoxetine treatment. Baseline increases in compulsive grooming and impairments in reversal learning in KOs improve after fluoxetine treatment. Additionally, *Sapap3*-KOs display distinct patterns of abnormal LOFC activity during grooming and reversal learning, both of which normalize after fluoxetine. Finally, we show that encoding of reversal learning and compulsive behavior by individual LOFC neurons is independent. Consequently, disrupted LOFC encoding of reversal learning is distinct from and independent of encoding of compulsive grooming in *Sapap3*-KO mice.

Methods

Animals: All procedures were carried out in accordance with the guidelines for care and use of laboratory animals from the NIH and with approval from the University of Pittsburgh Institutional Animal Care and Use Committee (IACUC). *Sapap3*-KOs (n = 8; 5 female) and WT (n = 6; 3 female) littermates were maintained on a C57BL/6 background. Mice were group-housed with 2–5 same-sex mice per cage in reverse light cycle (12:12, lights on at 7pm) with *ad libitum* access to food and water, except during operant training when food was restricted. All tests were conducted under red or infrared lighting during dark cycle.

Calcium imaging surgery: Mice underwent two surgeries for optical imaging studies similar to standard protocols (*28, 29*). For the first surgery, 800nl of a virus encoding GCaMP6f under the synapsin promotor (AAV5-synapsin-GCaMP6f-WPRE-SV40, titer 1.82×10^{12}; Penn Vector Core) was injected into the LOFC (AP: +2.7, ML: -1.0, DV: -1.6), followed by implantation of a gradient refractive index lens (ProView GRIN lens, 6mm long x 0.5mm wide; Inscopix, Palo Alto, CA USA) dorsal to the viral injection target (AP: +2.6, ML: -1.2, DV: -1.4). After 3-4 weeks of virus expression, a magnetic microscope baseplate (Inscopix) was implanted to allow attachment of the miniature microscope (nVista 2.0, Inscopix). More details can be found in the Supplement. Lens placements for individual animals are shown in Fig.S1.

Fluoxetine administration: (±)Fluoxetine hydrochloride (Fluoxetine; NIMH Chemical Synthesis and Drug Supply Program) was administered via drinking water according to established methods (*30*). 100mg/L fluoxetine hydrochloride was administered for 4 weeks to achieve a target dose of 18mg/kg, followed by a 2-week drug washout period (*31*).

Experimental design: Behavior and neural data were collected weekly for grooming and every other week for reversal learning (Fig.1b). In weeks where both behaviors were tested, grooming assessment was conducted first, and mice underwent operant training for 2 days prior to reversal imaging on the third day (details below). Neural and behavior data are presented from baseline and 4-week treatment sessions, and behavior data is also presented from the reversal learning washout session.

Grooming imaging procedures: Mice were tested in a clear acrylic chamber (8”x8”x12”) positioned above a behavior acquisition camera (Fig.1a; Point Grey Blackfly, FLIR Integrated Imaging Solutions, 40Hz). Behavior video and calcium signals were synchronized by a central data acquisition box (LabJack U3-LV, Labjack Corporation, Lakewood CO USA). Neural and behavior data were recorded for 40 minutes. Videos were analyzed offline by a trained experimenter blind to genotype and treatment using Observer XT software (Noldus, Leesburg, VA). Frame-by-frame analysis was used to identify the start and end of face and body grooming and hind-leg scratching (more details available in Supplement).

Operant conditioning imaging procedures and analysis: Mice were tested in a reversal learning paradigm using operant chambers (Med Associates, Fairfax, VT) similar to previously described (*24*) with modifications for imaging studies (see Supplement). Mice were pretrained on the task, and for each timepoint they were tested for three days. The first two days used the same rule (e.g. left lever correct, right lever incorrect, using the contingency from their most recent prior test), and on the third day the contingency was reversed (e.g. right lever correct) and calcium imaging was performed. Mice were trained on a variable ratio (VR) 2 schedule, and rewarded correct responses resulted in retraction of the two levers and delivery of a reward pellet. Operant behavior events and calcium signals were synchronized via TTL pulses from MED-PC system and frame information from Inscopix sent directly to a central data acquisition box (Labjack). Neural data and behavior were recorded for 30 minutes. Time to acquire the correct lever press was estimated by the mid-point of the sigmoid (1) fit to the cumulative distribution of correct lever presses. In the formula, A and B are the slope and midpoint of the sigmoid, respectively.

$$f(x) = \frac{1}{(1+ e^{-A*(x-B)})} \quad (1)$$

Imaging acquisition, processing and analysis: nVistaHD software recorded fluorescent signal as compressed greyscale tiffs (20Hz, 470nm LED power 0.1-0.3mW, image sensor gain = 1-4). All imaging pre-processing was performed using Mosaic software (version 1.2.0, Inscopix) via custom Matlab (MATHWORKS, Natick MA, USA) scripts. Data were decompressed, downsampled (x4 spatial and x2 temporal), and motion corrected before fluorescent signals were extracted from individual neurons using Constrained Nonnegative Matrix Factorization for Endoscopic data (CNMFe) (*32*), with putative neurons manually sorted by blind observer (*28*).

Longitudinal tracking of neurons across sessions: Putative neurons identified via CNMFe were matched across sessions using *CellReg* (*33*). More details are available in the Supplement.

Encoding model: To determine the extent to which grooming or reversal learning events were encoded in LOFC neurons, we modified a previously described multiple linear regression encoding model (*34*). More details are available in the Supplement.

Statistical analysis: Effects of genotype and fluoxetine on behavior were assessed using repeated measures ANOVA. Percentages of cells modulated and strength of encoding were assessed using repeated measures ANOVA and linear regression, respectively. Reversal learning imaging metrics were adjusted for differences in the number of behavioral events. Plots of reversal learning imaging metrics display residuals after correcting for differences in the number of behavioral events. Description of analysis of expected versus actual overlap between grooming and reversal learning can be found in the Supplement. Graphs show individual datapoints and SEM unless otherwise stated.

Results

Analysis of grooming behavior

Sapap3-KOs groomed for a larger percentage of time both at baseline and after 4 weeks of fluoxetine treatment (Fig.1c; genotype: $F_{(1,12)} = 8.5$,$p = 0.01$; drug: $F_{(1,12)} = 0.08$, $p = 0.79$; genotype x drug: $F_{(1,12)} = 0.02$, $p = 0.88$). In contrast, baseline increases in the number of grooming bouts in KOs normalized after fluoxetine treatment (Fig.1d; genotype: $F_{(1,12)} = 13.5$, $p = 0.003$; drug: $F_{(1,12)} = 8.8$, $p = 0.01$; genotype x drug: $F_{(1,12)} = 6.0$, $p = 0.03$). KOs engaged in longer grooming bouts compared to WTs, which was apparent across all bout lengths (Fig.1e; $p < 0.001$). The number of bouts, but not the total time grooming, decreased after fluoxetine because the length of grooming bouts significantly increased after fluoxetine in both WTs (Fig.1f) and KOs (Fig.1g).

Neural activity during grooming

To determine whether LOFC neurons were modulated during grooming, we analyzed *in vivo* calcium imaging data (Fig.2a-c) by adapting a previously described linear regression model (*34*) (see Supplement; Fig.2d). This approach allowed us to quantify how well LOFC neurons encode grooming using two different metrics: 1) the percentage of LOFC neurons that significantly encode grooming, and 2) the strength of encoding in each significantly modulated neuron. First, we assessed the total population of cells (Fig.2e; Table 1). In KOs, baseline increases in the percentage of LOFC neurons inhibited during grooming ($groom_{inh}$) normalized after fluoxetine (Fig.2f; genotype: $F_{(1,12)} = 6.90$, $p = 0.02$; drug: $F_{(1,12)} > 100$, $p < 0.001$; drug x genotype: $F_{(1,12)} > 100$, $p < 0.001$). Both at baseline and after fluoxetine, similar percentages of LOFC neurons from KOs and WTs were excited during grooming ($groom_{exc}$) (Fig.2g). Additionally, both $groom_{inh}$ (Fig.2h) and $groom_{exc}$ (Fig.2i) neurons from KOs encoded grooming more strongly than neurons from WTs both at baseline and after fluoxetine. Interestingly, while the percentage of $groom_{inh}$ neurons did not correlate with the number of grooming bouts at baseline in KOs or WTs (Fig.2j), the fluoxetine-associated decrease in the percentage of $groom_{inh}$ neurons significantly correlated with a decrease in the number of grooming bouts in KOs but not WTs (Fig.2k; KO: $r = 0.80$, $p = 0.01$; WT: $r = 0.40$, $p = 0.41$). Consequently, fluoxetine-associated decreases in the percentage of $groom_{inh}$ LOFC neurons predicted decreases in grooming in KOs.

Decreases in the percentage of $groom_{inh}$ LOFC neurons after fluoxetine treatment could arise in two ways – fewer neurons could remain inhibited and/or fewer new neurons could become inhibited. To test these two possibilities, the same neurons were tracked across grooming sessions (see Methods; Table 2). Much like the untracked dataset (Fig.2), there was a significantly higher baseline percentage of $groom_{inh}$ neurons in KOs that decreased after fluoxetine treatment (Fig.3a,b). While there were no genotype differences in the percentage of neurons that *remained* inhibited during grooming after fluoxetine (Fig.3c), fewer LOFC neurons *became* newly inhibited during grooming in KOs (Fig.3d; $p < 0.001$). Therefore, fluoxetine-associated decreases in the percentage of $groom_{inh}$ neurons in KOs are due to fewer neurons becoming inhibited after fluoxetine treatment.

Analysis of reversal-learning behavior

We next assessed the patterns of neural activity associated with reversal learning. Mice were first trained to associate one of two levers with reward on a VR2 schedule as previously described (*24*) (see Methods; Figs.4a,b). Fluoxetine normalized baseline reductions in the number of correct lever presses (Fig.4c; genotype: $F_{(1,12)} = 5.72$, $p = 0.03$; drug: $F_{(1,12)} = 0.76$, $p = 0.39$; genotype x drug: $F_{(1,12)} = 4.55$, $p = 0.04$) and increases in time to acquire the correct lever (see Methods; Fig.4d,e; genotype: $F_{(1,12)} = 10.01$, $p = 0.008$; drug: $F_{(1,12)} = 1.31$,$p = 0.25$; genotype x drug: $F_{(1,12)} = 6.87$, $p = 0.02$) in KOs. Since correct lever presses trigger reward delivery and the start of the next trial, significant baseline reductions in the number rewards received (Fig.4f) and trials completed (Fig.S2a) also normalized after fluoxetine in KOs. Additionally, KO and WT mice showed similar significant decreases in incorrect lever presses after fluoxetine (Fig.4g). No genotype- or fluoxetine-associated differences in the number of total (Fig.S2b) or unrewarded (Fig.S2c) magazine entries were observed.

To determine whether differences in behavior following 4 weeks of fluoxetine treatment were due to drug versus additional training on the task, reversal learning was repeated after a 2-week fluoxetine

washout period. After washout, the number of correct lever presses significantly decreased (Fig.S3a) and the time to acquire correct presses significantly increased (Fig.S3b), indicating prior improvements in reversal learning were due to fluoxetine. In contrast, decreases in the number of incorrect lever presses were still observed after washout in both genotypes (Fig.S3d), suggesting that these changes were likely due additional training. Together, these analyses indicate that baseline behavioral deficits in reversal learning in KOs normalized due to fluoxetine treatment.

Neural activity during reversal learning

We next determined how LOFC neurons encoded information relevant to the reversal learning task using a variant of the linear regression model described above. In this model, five behavioral variables – three actions (correct lever presses, incorrect lever presses and magazine entries) and two sensory stimuli (reward cues and trial start cues) – were used to predict each cell's calcium signal (Figs.5b-d). Notably, there were no genotype- or fluoxetine-associated differences in the percentage of cells excited in response to any of the five behavioral variables (Fig.5e-g, Fig.S4a,b) (few neurons were inhibited by task events and consequently were not included in these analyses). In contrast, baseline deficits were observed in the strength of encoding of both correct lever presses (Fig.5h; genotype: $p = 0.01$; drug: $p = 0.18$; genotype x drug: $p = 0.04$) and the reward cue (Fig.5i; genotype: $p = 0.001$; drug: $p = 0.45$; genotype x drug: $p = 0.01$) in KOs; these deficits were normalized after fluoxetine treatment. Encoding of correct lever presses and reward cue and changes following fluoxetine did not correlate with the time to acquire correct lever presses after reversal (Fig.S5). Additionally, deficits in encoding of the reward cue were unlikely to be due to a generalized sensory processing deficit as there was no genotype- or fluoxetine-associated difference in coding of the trial start cue (Fig.S4c). The strength of encoding of the incorrect lever press (Fig.5j) significantly decreased after fluoxetine treatment in both WTs and KOs. Finally, there were no genotype- or fluoxetine-associated differences in the encoding of magazine entries (Figs.S4d). Therefore, fluoxetine-associated improvements in reversal learning in KOs were associated with improvements in the strength of encoding of correct lever presses and the reward cue.

Interaction of LOFC neural activity during grooming and reversal learning

We next sought to determine how these behaviors interact. We first examined our behavioral data. Performance on the reversal learning task did not correlate with grooming levels, similar to our prior observations (*24*) and those of other groups (*25, 27*) (Fig.S6). Next, we assessed the overlap between neurons that encode reversal learning and neurons that encode compulsive grooming. LOFC neurons were tracked between grooming and reversal learning sessions at both the pre- and post- fluoxetine time points (Fig.7b-c) and pooled across animals of the same genotype to improve statistical power (see Supplement; Figs. 6a,f; Table 2). To determine whether the actual overlap between reversal learning and grooming-encoding cells was different from that which would be expected by chance, we performed a bootstrap analysis (see Supplement). For both pre- and post- fluoxetine, the actual overlap between cells encoding the five reversal learning parameters and grooming fell within the 95% confidence intervals of the overlap expected by chance for nearly all comparisons except for overlap between $groom_{inh}$ neurons and neurons encoding the incorrect press pre-fluoxetine (Figs.6c-e,h-j, Figs.S7b-c,e-f). These data indicate that cells encoding reversal learning are randomly distributed among cells encoding grooming (Fig.8a; e.g. are overlapping and/or segregated at the level expected by chance).

Finally, we analyzed whether encoding of grooming influenced the strength of encoding of reversal learning. Similar to the untracked dataset (Fig.5), tracked neurons in KOs showed deficits in the strength of encoding of both correct lever presses (Fig.7d) and reward cues (Fig.7g), which normalized after fluoxetine. Pre-fluoxetine, genotype differences in the strength of encoding were not influenced by whether a neuron encoded grooming, for either correct lever presses (Fig.7e; genotype: $p < 0.001$; groom modulation: $p = 0.01$; genotype x groom mod: $p = 0.56$) or reward cues (Fig.7h; genotype: $p = 0.1$; groom modulation: $p = 0.04$; genotype x groom mod: $p = 0.85$). Surprisingly, both pre- and post-fluoxetine, $groom_{inh}$ neurons from both WTs and KOs showed weaker encoding of correct lever presses (Fig.7e,f; pre-fluoxetine: post-hoc t-test groom inhib vs no modulation: $p = 0.01$; post-fluoxetine: post-hoc t-test groom inhib vs no modulation: $p = 0.001$) and reward cues (Fig.7h,i; pre-fluoxetine: post-hoc t-test groom inhib vs no modulation: $p = 0.03$; post-fluoxetine: post-hoc t-test groom inhib vs no modulation: $p = 0.04$) than neurons that were not modulated by grooming. Similarly, $groom_{inh}$ neurons also encoded magazine entries more weakly than

neurons that were not modulated by grooming in both genotypes (Fig.S8a-c). There were no effects of grooming-modulation on encoding of incorrect lever presses (Fig.S8d-f) or trial start cues (Fig.S8g-i). Therefore, degraded encoding of correct lever presses, reward cues and magazine entries in $groom_{inh}$ neurons is independent of genotype and fluoxetine treatment (Fig.8b). Thus, these results suggest that whether or not a neuron encodes grooming does not contribute to pathologic deficits in the encoding strength during reversal learning in KOs.

Discussion

Patients with OCD display disrupted performance during reversal learning tasks, yet whether these behaviors share common neural underpinnings is unknown. Here we replicate and extend prior work showing that *Sapap3*-KO mice display both compulsive behavior and deficits in reversal learning. While we demonstrate that both deficits improve with fluoxetine, the severity of compulsive grooming does not correlate with the extent of reversal learning deficits. Additionally, we provide several pieces of new evidence suggesting that reversal learning deficits and compulsive behaviors arise from disparate network abnormalities in the LOFC. First, compulsive grooming and deficits in reversal learning are associated with distinct patterns of abnormal LOFC activity, both of which normalize after fluoxetine treatment. During grooming, KO mice have a higher percentage of inhibited LOFC neurons, while during reversal learning, KO mice show weaker encoding of the correct lever press and reward cue, with no change in percentages of modulated cells. Second, these patterns of abnormal LOFC activity are independent of one another. We find that reversal learning-encoding neurons are distributed randomly among grooming-modulated neurons. Additionally, the presence of grooming encoding does not contribute to the weaker encoding of reversal learning information observed in KO mice. Taken together, these data indicate that the LOFC plays both independent and distinct roles in these two pathological behaviors and their improvement with fluoxetine.

Our *in vivo* calcium imaging data suggest that LOFC neurons display heterogeneous excitatory and inhibitory responses to normal grooming in WT mice, and that the specific changes in activity that contribute to pathologic grooming arise from a preponderance of $groom_{inh}$ neurons in KOs. Additionally, our data showing that reductions in grooming are correlated with fluoxetine-associated decreases in $groom_{inh}$ neurons, support an emerging model in which interventions that boost LOFC activity in *Sapap3*-KOs lead to decreases in grooming (*15*). How might these subpopulations of $groom_{inh}$ neurons arise? We propose that decreases in activity in $groom_{inh}$ neurons are most likely due to decreases in the excitatory drive (as opposed to an increase in inhibitory drive to $groom_{inh}$ neurons), as post-mortem data from patients with OCD show a decrease in a variety of transcripts associated with excitatory, but not inhibitory synapses, including *SAPAP3* (*23*). It is also possible that these decreases in excitation stem from sources extrinsic to the LOFC. Given that patients with OCD show hyperactivity in cortical-striatal-thalamo-cortical circuits (*11-13*), at first glance it seems likely that LOFC neurons receive increased, not decreased, inputs from the thalamus, suggesting that reductions in input may arise from other cortical or subcortical areas such as the amygdala. However, we cannot rule out the possibility that $groom_{inh}$ neurons receive increased inhibition during grooming from local interneurons (*26*). Future studies measuring grooming-related activity selectively in GABAergic interneurons or excitatory neurons that receive inputs from specific areas will be necessary to understand the drivers of the heterogeneous grooming-related activity that we find here.

By taking advantage of the ability to track the same neurons over time, we also begin to elucidate how fluoxetine changes the encoding properties of LOFC neurons. Neurons can belong to one of three populations with respect to encoding of grooming after fluoxetine: they can remain modulated; they can stop being modulated; and they can become newly modulated. We find that fluoxetine specifically decreases the percentage of new $groom_{inh}$ indicating subpopulations of LOFC neurons respond differentially to SSRI administration. Because serotonin is increased broadly following systemic fluoxetine administration, it remains unknown whether differential effects of serotonin are due to local effects on the excitability of LOFC subpopulations or whether serotonin modulates other brain areas that preferentially project to subsets of LOFC neurons. As a caveat, we are unable to address the stability of grooming encoding in the absence of fluoxetine or the time frame by which new neurons are added and old neurons drop out of the grooming ensemble as we only measured activity at two time points: pre- and post- fluoxetine.

In addition to assessing compulsive grooming, we explored the neural correlates of reversal learning, and found that fluoxetine-associated increases in the strength of encoding of correct lever presses and the reward cue by individual LOFC neurons in KO mice parallel improvements in baseline reversal learning deficits. One benefit of our task design is that mice are trained on a VR2 schedule, which allows for the dissociation of neurons associated with the action of the lever press from the sensory cues associated with the reward. As a result, deficits in encoding of reversal learning may arise due to disruptions with associating the correct lever press with the reward cue. While the necessity of the LOFC in reversal learning tasks is controversial (*35, 36*), it is likely involved in mediating the impact of serotonin on reversal learning, as depletion of serotonin in the LOFC is sufficient to disrupt reversal learning (*37*). While we did not directly assess the necessity of the LOFC for fluoxetine-associated improvements, our calcium imaging data suggest that the LOFC is involved in the normalization of behavior after fluoxetine. Additionally, we cannot assess how value is encoded in LOFC neurons given the deterministic nature of the current design, or whether neurons representing correct/incorrect lever presses encode that specific lever or rewarded/unrewarded actions in general. Future task designs in which rewards are probabilistic and contingencies switch multiple times during a single session will be better able to address these limitations.

If disrupted reversal learning and compulsive behaviors arise from distinct and independent coding deficits in the LOFC, what can we conclude about the association between abnormal cognitive flexibility and OCD? Our data may help to reconcile competing interpretations of prior work showing that both patients with OCD and their unaffected relatives have abnormal OFC activity during reversal learning (*9*). One interpretation is that abnormal OFC activity during reversal learning may constitute an OCD endophenotype and provide a causal and quantifiable link between genetic susceptibility and the symptoms of OCD (*38*). A second is that, because abnormal OFC activity of unaffected relatives is dissociable from compulsive behaviors, deficits in reversal learning are separable from compulsive behaviors. In this interpretation, OCD risk genes cause a variety of molecular and circuit-level changes: one subset of changes leads to the symptoms of OCD while a separate subset leads to deficits in reversal learning that may impact functioning independent of obsessions and compulsions. The data we report here support the second interpretation – that deficits in reversal learning are unrelated to compulsive behaviors – since they arise from distinct and independent coding deficits.

Acknowledgments:
We would like to thank Xiaojun Li, Brittany Chamberlain and Alexander Lammers for help with video scoring; Drs Jesse Wood, Zoe LaPalombara and James Hyde for help with data processing pipeline development; and the rest of the Ahmari lab for helpful feedback. This work was supported by NIMH R21 MH116330, Burroughs Wellcome CAMS Award, NIMH BRAINS R01MH104255, McKnight Scholar Award, MQ Fellows Award, and Klingenstein-Simons Fellowship Award in the Neurosciences to SEA.

Tables

Table 1: Number of cells across mice

Animal	Genotype	Pre Grooming	Post Grooming	Pre Reversal	Post Reversal
3001	WT	128	117	131	109
3297	WT	57	68	77	89
3298	WT	111	84	108	91
3592	WT	106	72	70	101
3604	WT	137	103	133	107
3632	WT	109	112	62	118
Avg ± SEM	WT	108 ± 28	93 ± 21	97 ± 31	103 ± 11

Animal	Genotype	Pre Grooming	Post Grooming	Pre Reversal	Post Reversal
2991	KO	127	134	122	123
2993	KO	116	131	71	109
3091	KO	180	107	84	141
3605	KO	124	129	106	149
3616	KO	153	136	108	142
3617	KO	133	139	144	123
3626	KO	88	64	74	69
3627	KO	81	38	59	56
Avg ± SEM	KO	125 ± 32	110 ± 38	96 ± 29	114 ± 34

Table 2: Number of tracked cells across mice

Animal	Genotype	Pre/Post Grooming	Pre Grooming/Reversal	Post Grooming/Reversal
3001	WT	86	62	78
3297	WT	39	49	45
3298	WT	56	88	57
3592	WT	50	56	52
3604	WT	81	99	81
3632	WT	64	48	89
Avg ± SEM	WT	63 ± 18	67 ± 21	67 ± 18

Animal	Genotype	Pre/Post Grooming	Pre Grooming/Reversal	Post Grooming/Reversal
2991	KO	88	90	101
2993	KO	74	55	93
3091	KO	92	71	98
3605	KO	79	78	87
3616	KO	72	91	103
3617	KO	67	97	80
3626	KO	0	51	52
3627	KO	34	44	28
Avg ± SEM	KO	63 ± 31	72 ± 20	80 ± 27

Figures

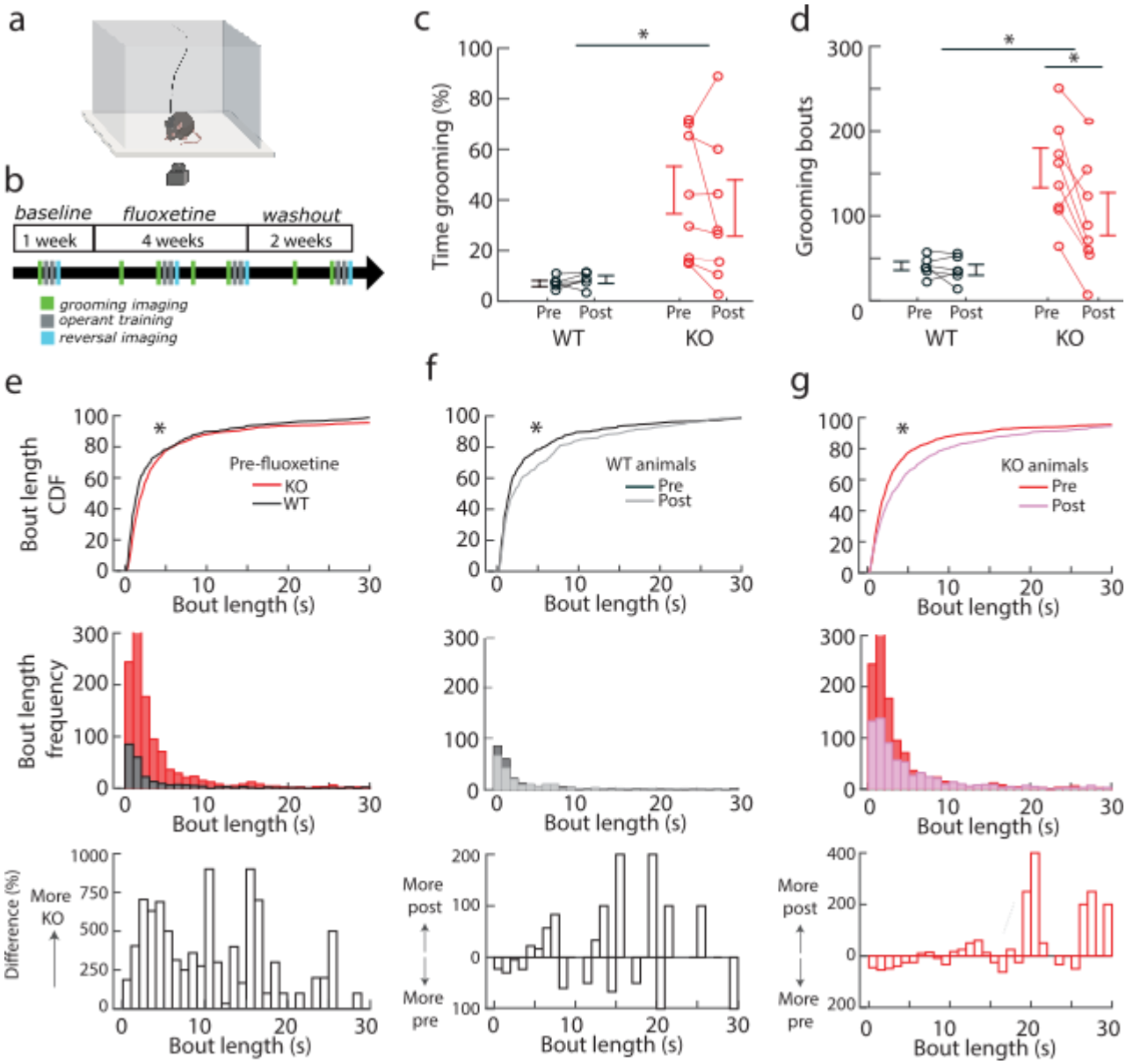

Figure 1: Baseline increases in the number of grooming bouts, but not total time grooming, normalize after fluoxetine treatment in KOs. (a) Grooming was tested in a clear acrylic chamber positioned above a behavior acquisition camera. (b) Experimental timeline: Baseline grooming (green) and reversal learning (cyan) were measured prior to 4 weeks of fluoxetine treatment. While fluoxetine was administered, grooming and reversal learning were assessed weekly and every 2 weeks, respectively. Post-fluoxetine data presented throughout the manuscript are from the 4-week time point. Grooming and reversal learning were also assessed after a 2 week washout period. (c) Data collected from 8 KO mice (red) and 6 WT littermates (black). Both pre- and post- fluoxetine, KOs spent more time grooming than WTs (genotype: $F_{(1,12)} = 8.5$,$p = 0.01$; drug: $F_{(1,12)} = 0.08$, $p = 0.79$; genotype x drug: $F_{(1,12)} = 0.02$, $p = 0.88$). (d) Pre-fluoxetine increases in the number of grooming bouts in KOs decrease after fluoxetine (genotype: $F_{(1,12)} = 13.5$, $p = 0.003$; drug: $F_{(1,12)} = 8.8$, $p = 0.01$; genotype x drug: $F_{(1,12)} = 6.0$, $p = 0.03$). (e-g) Differences in bout length between (e) WTs and KOs prior to fluoxetine treatment; (f) WTs pre- and post- fluoxetine; and (g) KOs pre- and post- fluoxetine. *Top*: Cumulative distribution function (CDF) of bout length. *Middle*: Histogram of bout length. *Bottom*: Percent difference in bout length frequency. (e) Bout lengths are longer in KOs compared with WTs (KS – $p < 0.05$). (f-g) Fluoxetine increases the length of grooming bouts in WTs (e; KS – $p < 0.05$) and KOs (f; KS – $p < 0.05$).

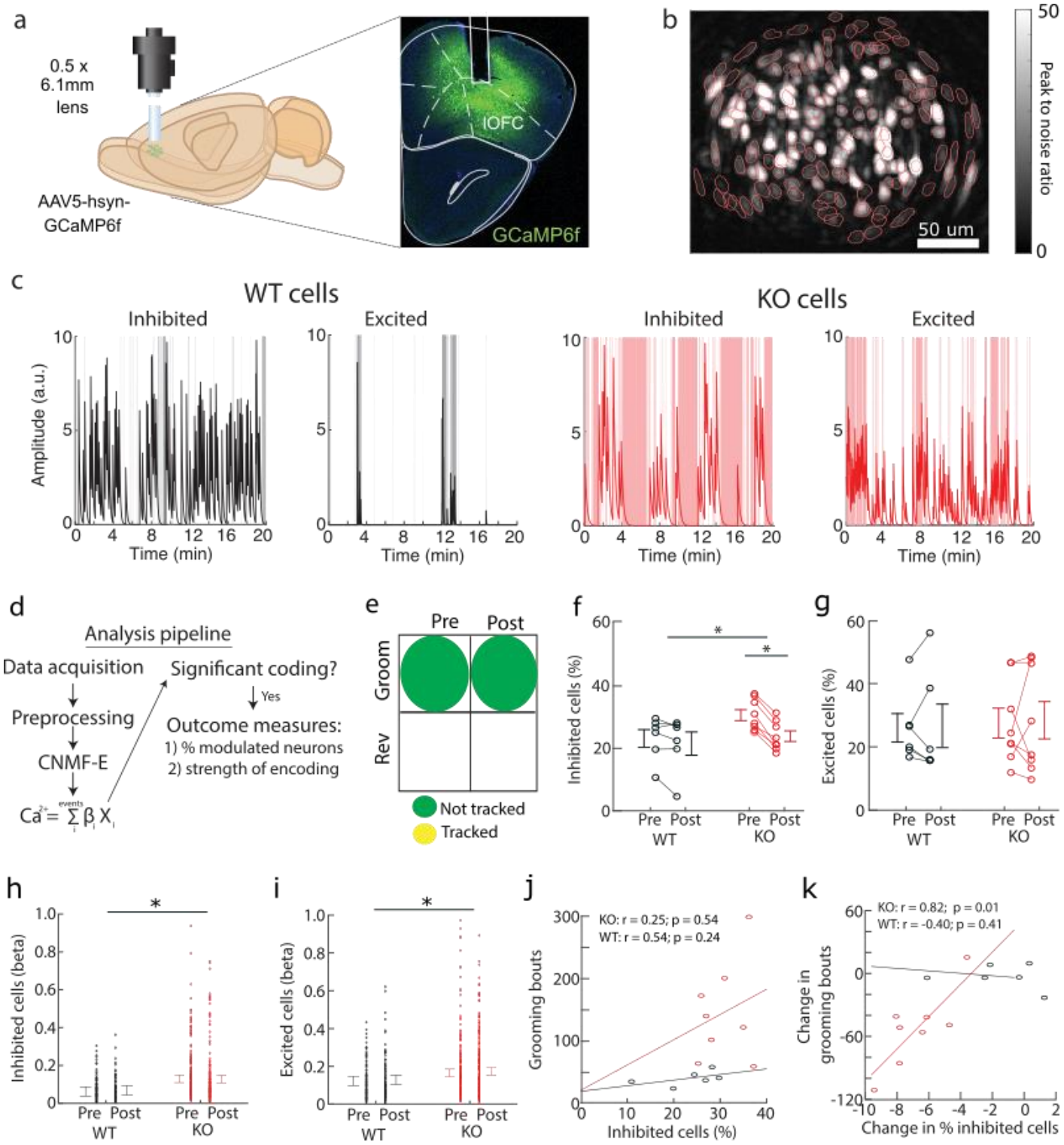

Figure 2: Fluoxetine-associated decreases in the number of grooming bouts are correlated with a decrease in the percentage of cells inhibited by grooming in KOs. (a) *Left:* Schematic of calcium imaging in the LOFC. *Right:* Representative coronal section showing lens placement and GCaMP6f expression. (b) Individual contours of putative LOFC neurons (red) plotted on top of the peak-to-noise ratio image of cell activity (scale bar=50um). c) Examples of cells that most strongly encode grooming from each genotype (grooming periods are depicted by grey/red shaded background). (d) Analysis pipeline: After data were acquired and preprocessed, calcium transients from individual cells were identified using CMNFe. Presence of significant encoding of behavior was determined using encoding model. Two distinct measures of encoding were used: 1) the percent of neurons that significantly encode the behavior and 2) the strength of encoding of individual neurons (See Methods) (e): Cells are not tracked between pre- and post-

fluoxetine sessions in this analysis. (f-g) Percentage of cells modulated by grooming pre- and post-fluoxetine in WTs and KOs. (f) Pre-fluoxetine increases in the percentage of inhibited neurons in KOs decreased after fluoxetine (genotype: $F_{(1,12)} = 6.90$, $p = 0.02$; drug: $F_{(1,12)} > 100$, $p < 0.001$; drug x genotype: $F_{(1,12)} > 100$, $p < 0.001$). (g) There were no genotype or fluoxetine effects on the percentage of excited cells (genotype: $F_{(1,12)} = 0.05$, $p = 0.82$; drug: $F_{(1,12)} = 0.08$, $p = 0.78$; genotype x drug: $F_{(1,12)} = 0.003$, $p = 0.96$). (h-i) Beta weights for cells modulated by grooming pre- and post-fluoxetine in WTs and KOs. Increased encoding strength of grooming in KOs does not change after fluoxetine in (h) inhibited cells (genotype: $p < 0.001$; drug: $p = 0.67$; genotype x drug: $p = 0.59$) or (i) excited cells (genotype: $p < 0.001$; drug: 0.61; genotype x drug: $p = 0.52$). (j) No correlation between baseline number of grooming bouts and the percentage of inhibited cells. (k) Decreases in the number of grooming bouts after fluoxetine were correlated with decreases in the percentage of inhibited cells in KOs, but not WTs.

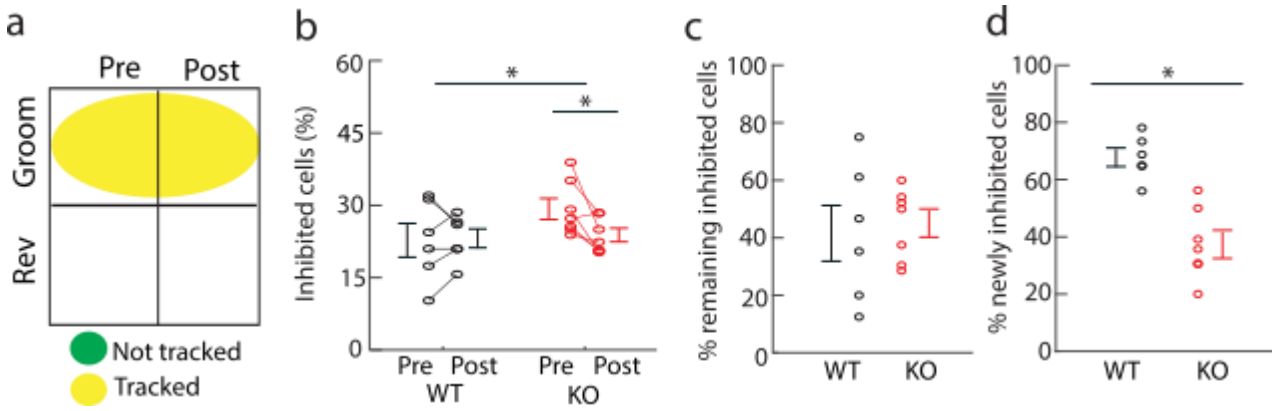

Figure 3: Decreased percentage of inhibited cells in KOs is due to fewer newly inhibited cells rather than fewer cells that remain inhibited after fluoxetine. (a) Cells tracked between pre- and post-fluoxetine grooming sessions. (b) Similar to the untracked dataset (Fig. 2), KOs show an increased percentage of grooming inhibited neurons that decreases after fluoxetine (genotype: $F_{(1,12)} = 5.03$, $p = 0.04$; drug: $F_{(1,12)} = 5.9$, $p = 0.03$; genotype x drug: $F_{(1,12)} = 5.1$, $p = 0.04$). (c) The percentage of neurons that remain inhibited by grooming after fluoxetine does not differ by genotype (t-test: $p = 0.54$). (d) Fewer new neurons become inhibited by grooming after fluoxetine in KOs compared with WTs (t-test: $p < 0.001$).

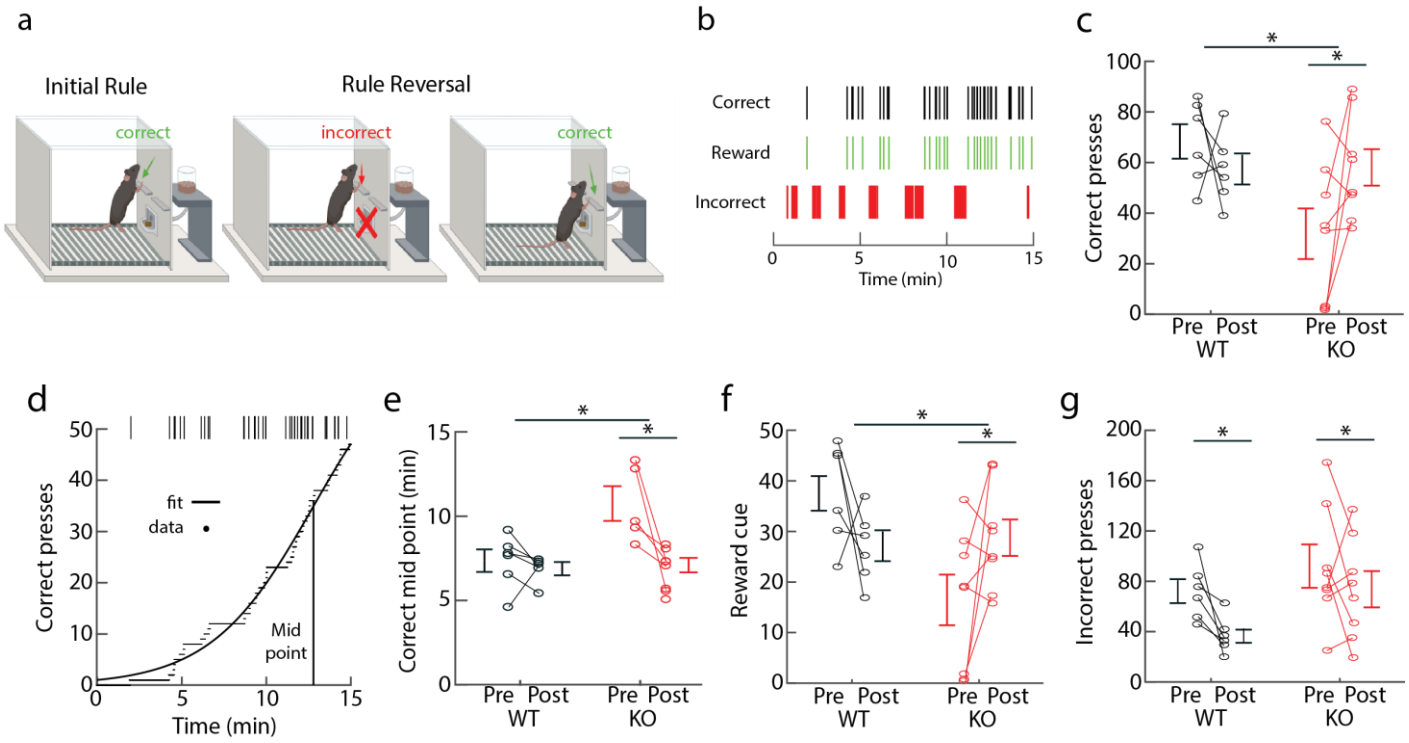

Figure 4: Baseline deficits in reversal learning in KOs improve after fluoxetine treatment. (a) Schematic of reversal learning task design. During operant training, mice associate one lever with reward. After reversal of lever contingencies, mice must learn that the other lever now delivers reward. (b) Example event raster of relevant events in the reversal learning task for one animal. (c) Decreases in the number of correct lever presses in KOs normalize after fluoxetine (genotype: $F_{(1,12)} = 5.72$, $p = 0.03$; drug: $F_{(1,12)} = 0.76$, $p = 0.39$; genotype x drug: $F_{(1,12)} = 4.55$, $p = 0.04$). (d) Example of fitting sigmoid to CDF of correct lever presses. The mid-point of the sigmoid is used as a measure of the time to acquire correct lever presses (See Methods). (e) Increases in the time to acquire the correct lever decrease after fluoxetine in KOs (genotype: $F_{(1,12)} = 10.01$, $p = 0.008$; drug: $F_{(1,12)} = 1.31$,$p = 0.25$; genotype x drug: $F_{(1,12)} = 6.87$, $p = 0.02$). (f) Because correct lever presses trigger rewards, decreases in the number of rewards in KOs also increase after fluoxetine (genotype: $F_{(1,12)} = 6.88$, $p = 0.02$; drug: $F_{(1,12)} = 0.04$, $p = 0.82$; genotype x drug: $F_{(1,12)} = 6.59$, $p = 0.02$). (g) The number of incorrect lever presses decreases after fluoxetine in both genotypes (genotypes: $F_{(1,12)} = 1.19$, $p = 0.30$; drug: $F_{(1,12)} = 8.87$, $p = 0.01$; genotype x drug: $F_{(1,12)} = 2.31$, $p = 0.15$).

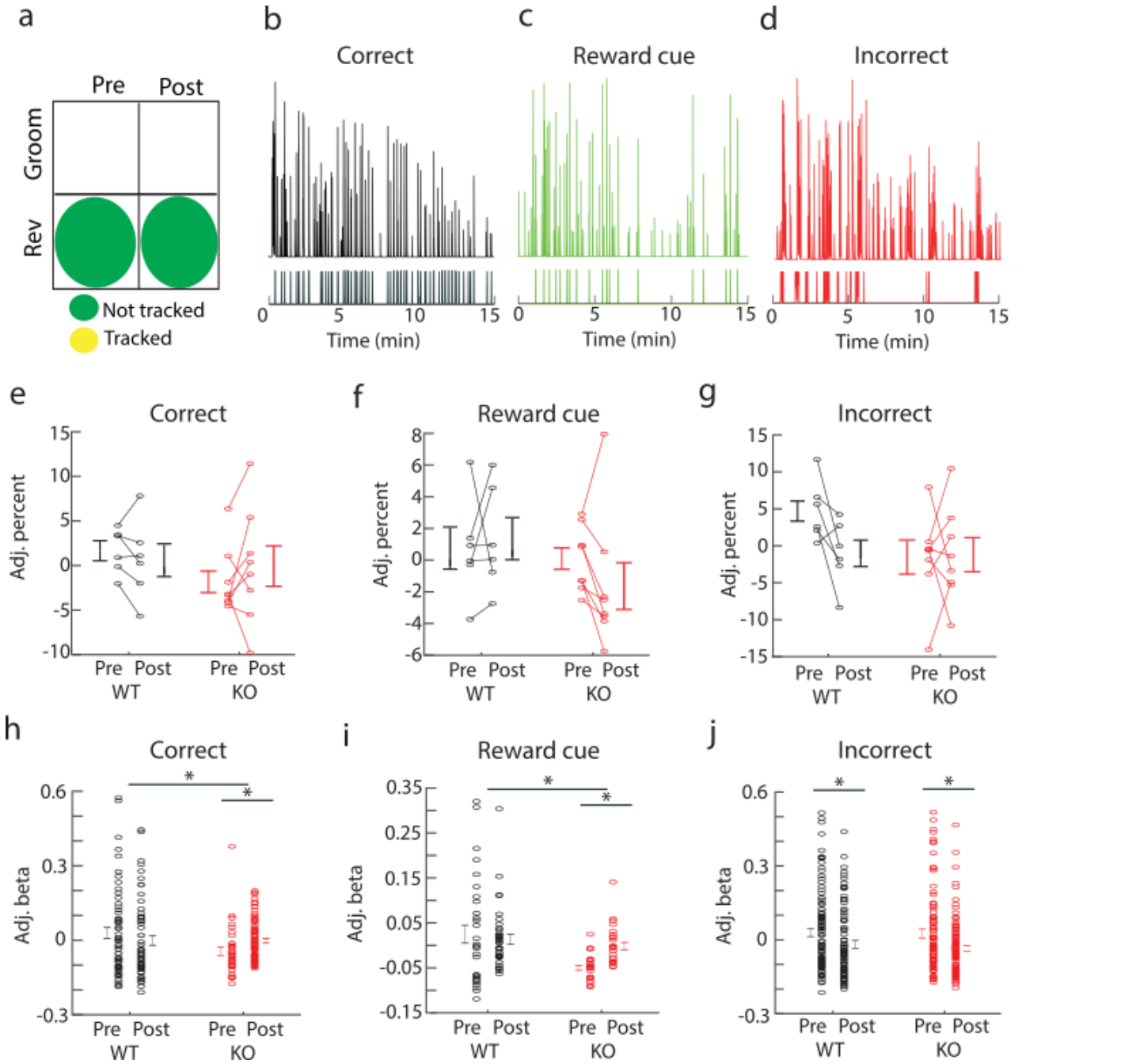

Figure 5: Baseline deficits in the strength of encoding of correct lever press and reward cue in LOFC neurons from KOs normalize after fluoxetine treatment. (a) Cells taken from the untracked dataset. (b-d) Examples of LOFC cells that best encode task relevant variables. *Top:* Example calcium traces. *Bottom:* Corresponding raster of behavioral events. (e-g) Percentages of modulated neurons were adjusted for the differences in the number of task events ("Adj. percent"). Plots display residuals after correcting for differences in the number of behavioral events. There were no genotype or fluoxetine effects on the percentage of neurons encoding (e) correct lever presses (genotype: $F_{(1,12)} = 0.77$, $p = 0.38$; drug: $F_{(1,12)} = 0.075$, $p = 0.78$; genotype x drug: $F_{(1,12)} = 1.3$, $p = 0.27$), (f) reward cues (genotype: $F_{(1,12)} = 1.49$, $p = 0.24$; drug: $F_{(1,12)} = 0.29$, $p = 0.60$; genotype x drug: $F_{(1,12)} = 1.34$, $p = 0.26$), or (g) incorrect lever presses (genotype: $F_{(1,12)} = 2.24$, $p = 0.16$; drug: $F_{(1,12)} = 2.02$, $p = 0.18$; genotype x drug: $F_{(1,12)} = 2.50$ $p = 0.14$). (h-j) Genotype and fluoxetine effects on the strength of encoding of task variables. Variables adjusted for number of task events and animal-to-animal variability ("Adj. beta"). Fluoxetine normalizes baseline reductions in the strength of encoding (h) correct lever presses (genotype: $p = 0.01$; drug: $p = 0.18$; genotype x drug: $p = 0.04$) and (i) reward cues (genotype: $p = 0.001$; drug: $p = 0.45$; genotype x drug: $p = 0.01$). (j) The strength of encoding of incorrect lever presses decreases after fluoxetine in both genotypes (genotype: $p = 0.65$; drug: $p = 0.01$; genotype x drug: $p = 0.43$).

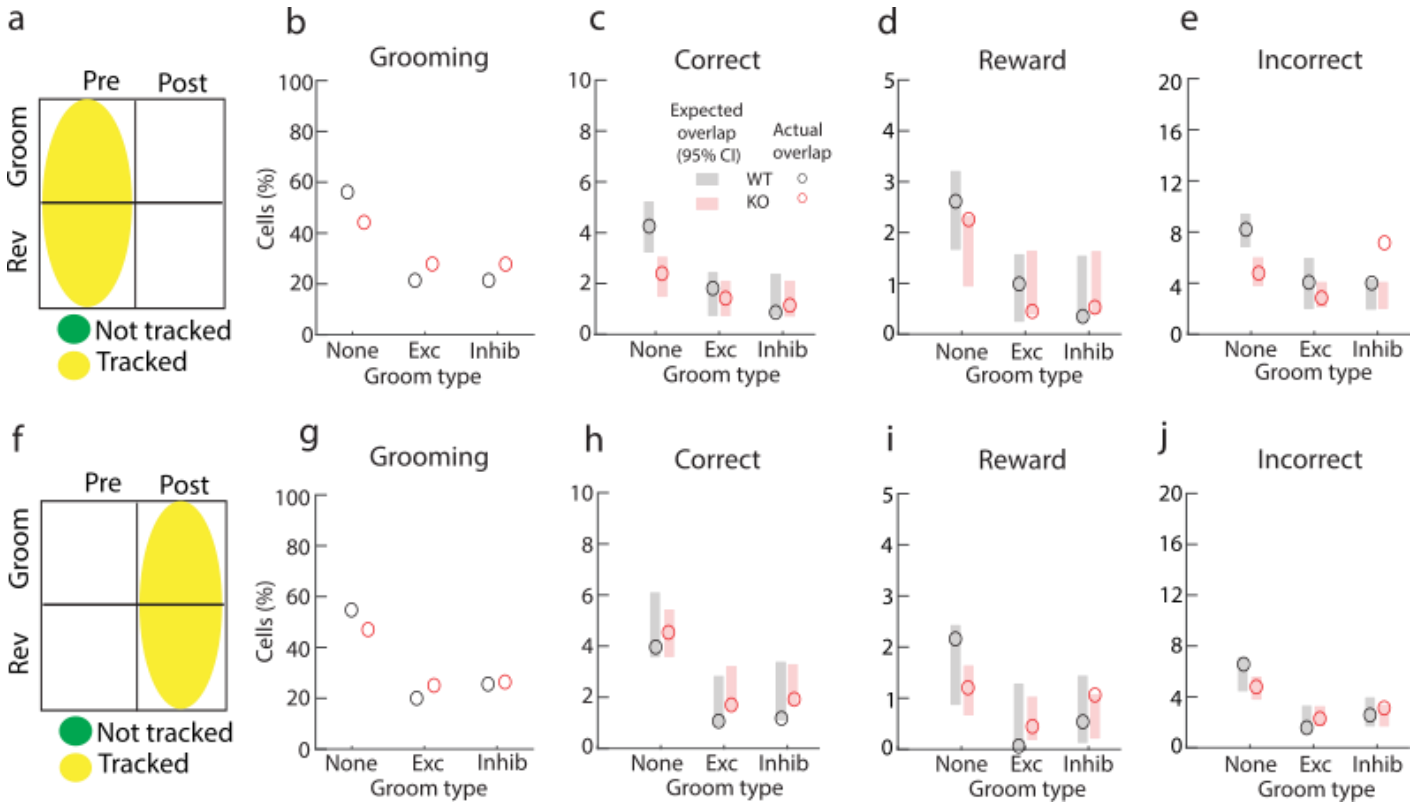

Figure 6: Reversal learning LOFC neurons are randomly distributed among grooming cells. (a) Cells were tracked between grooming and reversal sessions prior to fluoxetine. (b) Percentage of cells encoding grooming after pooling of all grooming cells across animals of the same genotype (WT black; KO red). Modified bootstrap analysis was performed (See Methods) to determine the expected overlap between populations encoding reversal learning and grooming. Populations were considered significantly overlapping or segregated if the actual overlap (circles) was above or below the 95% CI of the expected overlap (shaded rectangles), respectively. (c-e) Reversal learning cells are randomly distributed among grooming cells. Neurons encoding (b) correct lever presses, (d) Reward cues, and (e) incorrect lever presses are randomly distributed among grooming cells. The only exception is a greater than expected overlap between incorrect neurons and those inhibited by grooming. (f-j) Same as a-e but for cells tracked between post-fluoxetine grooming and reversal sessions.

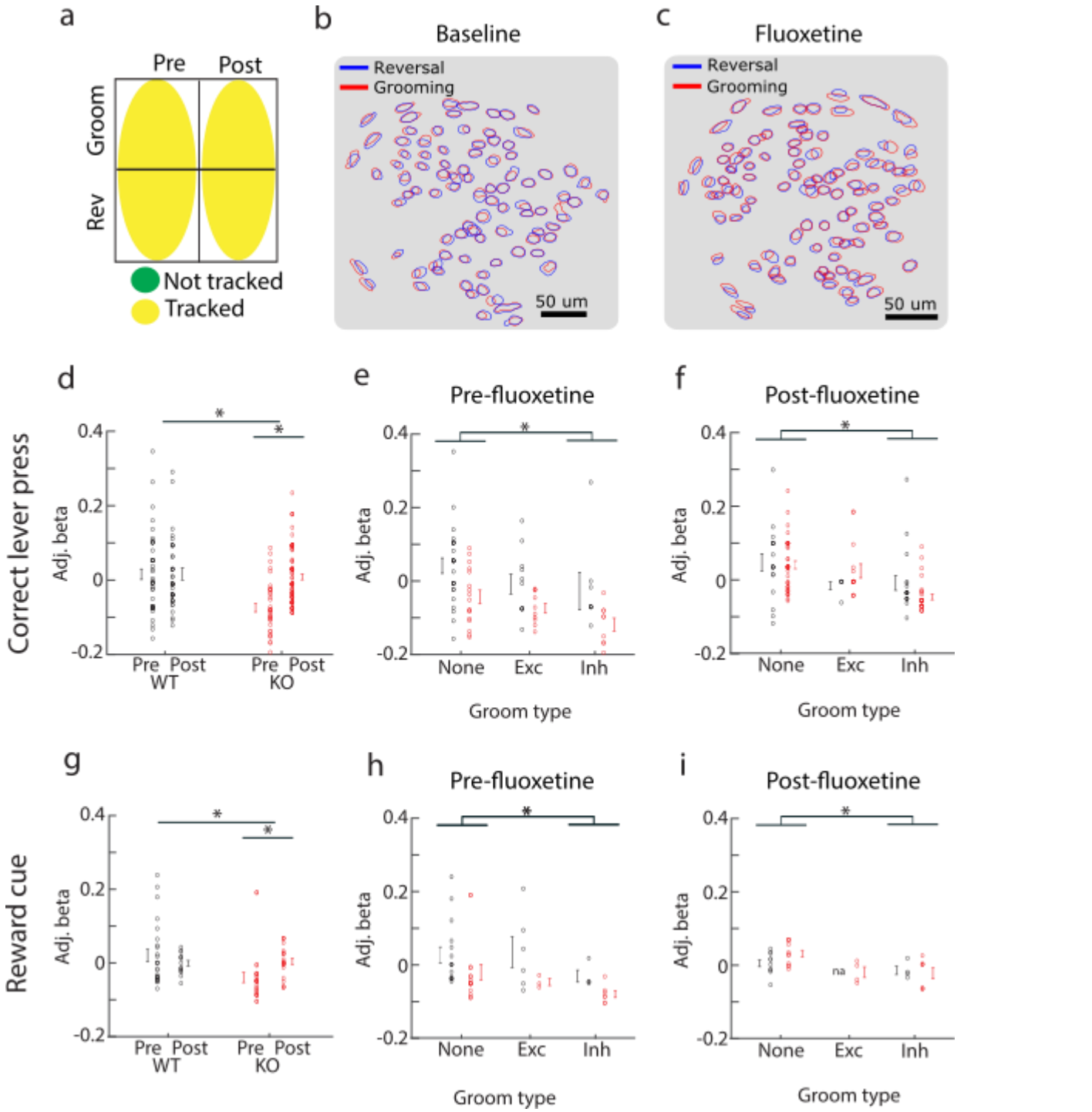

Figure 7: Presence of grooming encoding does not contribute to weaker encoding of reversal learning in KOs. (a) Cells are tracked between grooming and reversal sessions at both the pre- and post-fluoxetine time points. (b-c) Contour maps of putative LOFC neurons from a representative mouse aligned across reversal (blue) and grooming (red) sessions at baseline (left) and after 4 weeks of fluoxetine treatment (right). (d) Similar to Figure 5g, baseline deficits in encoding of correct lever presses normalize after fluoxetine in KOs (genotype: $p < 0.001$; drug: $p = 0.18$; genotype x drug: $p < 0.001$). (e) Presence of grooming encoding does not contribute to genotype differences (genotype: $p < 0.001$; groom modulation: $p = 0.01$; genotype x groom mod: $p = 0.56$; post-hoc t-test groom inhib vs no modulation: $p = 0.01$). However, cells inhibited by grooming in both genotypes encode correct lever press more weakly compared with cells not modulated by grooming. (f) Similar to (e) but post-fluoxetine treatment (genotype: $p = 0.67$; groom modulation: $p = 0.01$; genotype x groom mod: $p = 0.34$; post-hoc t-test groom inhib vs no modulation: $p = 0.001$). (g) Similar to Figure 5h, baseline deficits in encoding of reward cues normalize after fluoxetine in KOs (genotype: $p < 0.001$; drug: $p = 0.45$; genotype x drug: $p < 0.001$). (h) Prior to fluoxetine treatment,

cells inhibited by grooming in both genotypes encode reward cues more weakly compared with cells not modulated by grooming. However, presence of grooming encoding does not contribute to genotype differences (genotype: $p = 0.1$; groom modulation: $p = 0.04$; genotype x groom mod: $p = 0.85$; post-hoc t-test groom inhib vs no modulation: $p = 0.03$). (i) Similar to h but post-fluoxetine treatment (genotype: $p = 0.81$; groom modulation: $p = 0.03$; genotype x groom mod: $p = 0.73$; post-hoc t-test groom inhib vs no modulation: $p = 0.04$).

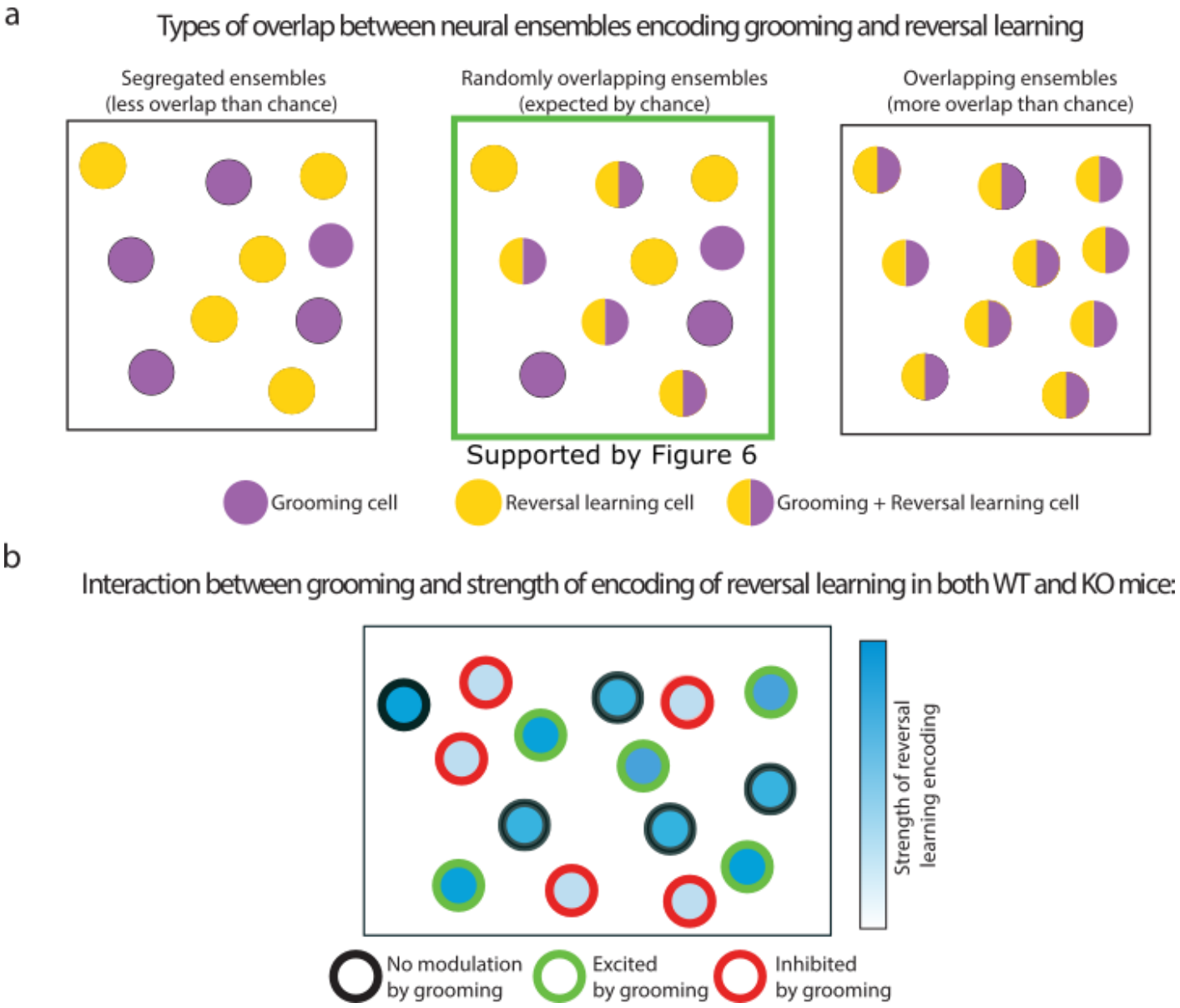

Figure 8: Summary of experimental evidence demonstrating that encoding of compulsive grooming and reversal learning is independent. (a) Grooming and reversal learning could overlap in 3 ways. Grooming and reversal learning cells could be part of separate (left), randomly overlapping (middle) or preferentially overlapping (right) ensembles. Data from Figure 6 suggests that grooming and reversal learning cells are randomly overlapping. (b) Grooming influences the strength of encoding of reversal learning information. In both WT and KO mice, neurons inhibited by grooming encode reversal learning more weakly than neurons that do not encode grooming. Because this interaction occurs in both genotypes and is not influenced by fluoxetine, it is not likely to contribute to pathology.

References

1. T. Endrass, S. Koehne, A. Riesel, N. Kathmann, Neural correlates of feedback processing in obsessive-compulsive disorder. *Journal of abnormal psychology* **122**, 387-396 (2013).
2. P. L. Remijnse *et al.*, Reduced orbitofrontal-striatal activity on a reversal learning task in obsessive-compulsive disorder. *Archives of general psychiatry* **63**, 1225-1236 (2006).
3. P. L. Remijnse *et al.*, Differential frontal-striatal and paralimbic activity during reversal learning in major depressive disorder and obsessive-compulsive disorder. *Psychological medicine* **39**, 1503-1518 (2009).
4. C. Szabó, A. Németh, S. Kéri, Ethical sensitivity in obsessive-compulsive disorder and generalized anxiety disorder: the role of reversal learning. *J Behav Ther Exp Psychiatry* **44**, 404-410 (2013).
5. G. Valerius, A. Lumpp, A. K. Kuelz, T. Freyer, U. Voderholzer, Reversal learning as a neuropsychological indicator for the neuropathology of obsessive compulsive disorder? A behavioral study. *J Neuropsychiatry Clin Neurosci* **20**, 210-218 (2008).
6. S. R. Chamberlain *et al.*, A neuropsychological comparison of obsessive-compulsive disorder and trichotillomania. *Neuropsychologia* **45**, 654-662 (2007).
7. H. W. Kim *et al.*, Further evidence of a dissociation between decision-making under ambiguity and decision-making under risk in obsessive-compulsive disorder. *J Affect Disord* **176**, 118-124 (2015).
8. S. Morein-Zamir *et al.*, The profile of executive function in OCD hoarders and hoarding disorder. *Psychiatry Res* **215**, 659-667 (2014).
9. S. R. Chamberlain *et al.*, Orbitofrontal dysfunction in patients with obsessive-compulsive disorder and their unaffected relatives. *Science* **321**, 421-422 (2008).
10. P. L. Remijnse *et al.*, Cognitive inflexibility in obsessive-compulsive disorder and major depression is associated with distinct neural correlates. *PloS one* **8**, e59600 (2013).
11. L. R. Baxter *et al.*, Local cerebral glucose metabolic rates in obsessive-compulsive disorder. A comparison with rates in unipolar depression and in normal controls. *Arch Gen Psychiatry* **44**, 211-218 (1987).
12. H. C. Breiter *et al.*, Functional magnetic resonance imaging of symptom provocation in obsessive-compulsive disorder. *Archives of general psychiatry* **53**, 595-606 (1996).
13. S. L. Rauch *et al.*, Regional cerebral blood flow measured during symptom provocation in obsessive-compulsive disorder using oxygen 15-labeled carbon dioxide and positron emission tomography. *Archives of general psychiatry* **51**, 62-70 (1994).
14. J. M. Welch *et al.*, Cortico-striatal synaptic defects and OCD-like behaviours in Sapap3-mutant mice. *Nature* **448**, 894-900 (2007).
15. E. Burguiere, P. Monteiro, G. Feng, A. M. Graybiel, Optogenetic stimulation of lateral orbitofronto-striatal pathway suppresses compulsive behaviors. *Science* **340**, 1243-1246 (2013).
16. K. K. Ade *et al.*, Increased Metabotropic Glutamate Receptor 5 Signaling Underlies Obsessive-Compulsive Disorder-like Behavioral and Striatal Circuit Abnormalities in Mice. *Biological psychiatry* **80**, 522-533 (2016).
17. J. M. Welch, D. Wang, G. Feng, Differential mRNA expression and protein localization of the SAP90/PSD-95-associated proteins (SAPAPs) in the nervous system of the mouse. *The Journal of comparative neurology* **472**, 24-39 (2004).
18. Y. Wan *et al.*, Circuit-selective striatal synaptic dysfunction in the Sapap3 knockout mouse model of obsessive-compulsive disorder. *Biological psychiatry* **75**, 623-630 (2014).
19. S. Zuchner *et al.*, Multiple rare SAPAP3 missense variants in trichotillomania and OCD. *Molecular psychiatry* **14**, 6-9 (2009).
20. M. Mattheisen *et al.*, Genome-wide association study in obsessive-compulsive disorder: results from the OCGAS. *Molecular psychiatry* **20**, 337-344 (2015).
21. S. E. Stewart *et al.*, Genome-wide association study of obsessive-compulsive disorder. *Mol Psychiatry* **18**, 788-798 (2013).
22. O. J. Bienvenu *et al.*, Sapap3 and pathological grooming in humans: Results from the OCD collaborative genetics study. *American journal of medical genetics. Part B, Neuropsychiatric genetics : the official publication of the International Society of Psychiatric Genetics* **150B**, 710-720 (2009).

23. S. C. Piantadosi, B. L. Chamberlain, J. R. Glausier, D. A. Lewis, S. E. Ahmari, Lower excitatory synaptic gene expression in orbitofrontal cortex and striatum in an initial study of subjects with obsessive compulsive disorder. *Molecular psychiatry*, (2019).
24. E. E. Manning, A. Y. Dombrovski, M. M. Torregrossa, S. E. Ahmari, Impaired instrumental reversal learning is associated with increased medial prefrontal cortex activity in Sapap3 knockout mouse model of compulsive behavior. *Neuropsychopharmacology : official publication of the American College of Neuropsychopharmacology* **44**, 1494-1504 (2019).
25. B. J. G. van den Boom, A. H. Mooij, I. Miseviciute, D. Denys, I. Willuhn, Behavioral flexibility in a mouse model for obsessive-compulsive disorder: Impaired Pavlovian reversal learning in SAPAP3 mutants. *Genes, brain, and behavior* **18**, e12557 (2019).
26. Z. Yang *et al.*, Dysfunction of Orbitofrontal GABAergic Interneurons Leads to Impaired Reversal Learning in a Mouse Model of Obsessive-Compulsive Disorder. *Curr Biol*, (2020).
27. N. Benzina, K. N'Diaye, A. Pelissolo, L. Mallet, E. Burguiere, A cross-species assessment of behavioral flexibility in compulsive disorders. *Commun Biol* **4**, 96 (2021).
28. S. L. Resendez *et al.*, Visualization of cortical, subcortical and deep brain neural circuit dynamics during naturalistic mammalian behavior with head-mounted microscopes and chronically implanted lenses. *Nature protocols* **11**, 566-597 (2016).
29. V. L. Corbit *et al.*, Dissociable roles of central striatum and anterior lateral motor area in initiating and sustaining naturalistic behavior. *bioRxiv*, 2020.2001.2008.899070 (2020).
30. S. E. Ahmari *et al.*, Repeated cortico-striatal stimulation generates persistent OCD-like behavior. *Science* **340**, 1234-1239 (2013).
31. S. C. Dulawa, K. A. Holick, B. Gundersen, R. Hen, Effects of chronic fluoxetine in animal models of anxiety and depression. *Neuropsychopharmacology : official publication of the American College of Neuropsychopharmacology* **29**, 1321-1330 (2004).
32. P. Zhou *et al.*, Efficient and accurate extraction of in vivo calcium signals from microendoscopic video data. *Elife* **7**, (2018).
33. L. Sheintuch *et al.*, Tracking the Same Neurons across Multiple Days in Ca. *Cell Rep* **21**, 1102-1115 (2017).
34. B. Engelhard *et al.*, Specialized coding of sensory, motor and cognitive variables in VTA dopamine neurons. *Nature* **570**, 509-513 (2019).
35. A. Izquierdo, J. L. Brigman, A. K. Radke, P. H. Rudebeck, A. Holmes, The neural basis of reversal learning: An updated perspective. *Neuroscience* **345**, 12-26 (2017).
36. T. A. Stalnaker, N. K. Cooch, G. Schoenbaum, What the orbitofrontal cortex does not do. *Nature neuroscience* **18**, 620-627 (2015).
37. J. Alsiö *et al.*, Serotonergic Innervations of the Orbitofrontal and Medial-prefrontal Cortices are Differentially Involved in Visual Discrimination and Reversal Learning in Rats. *Cereb Cortex*, (2020).
38. T. W. Robbins, M. M. Vaghi, P. Banca, Obsessive-Compulsive Disorder: Puzzles and Prospects. *Neuron* **102**, 27-47 (2019).

Supplemental Figures

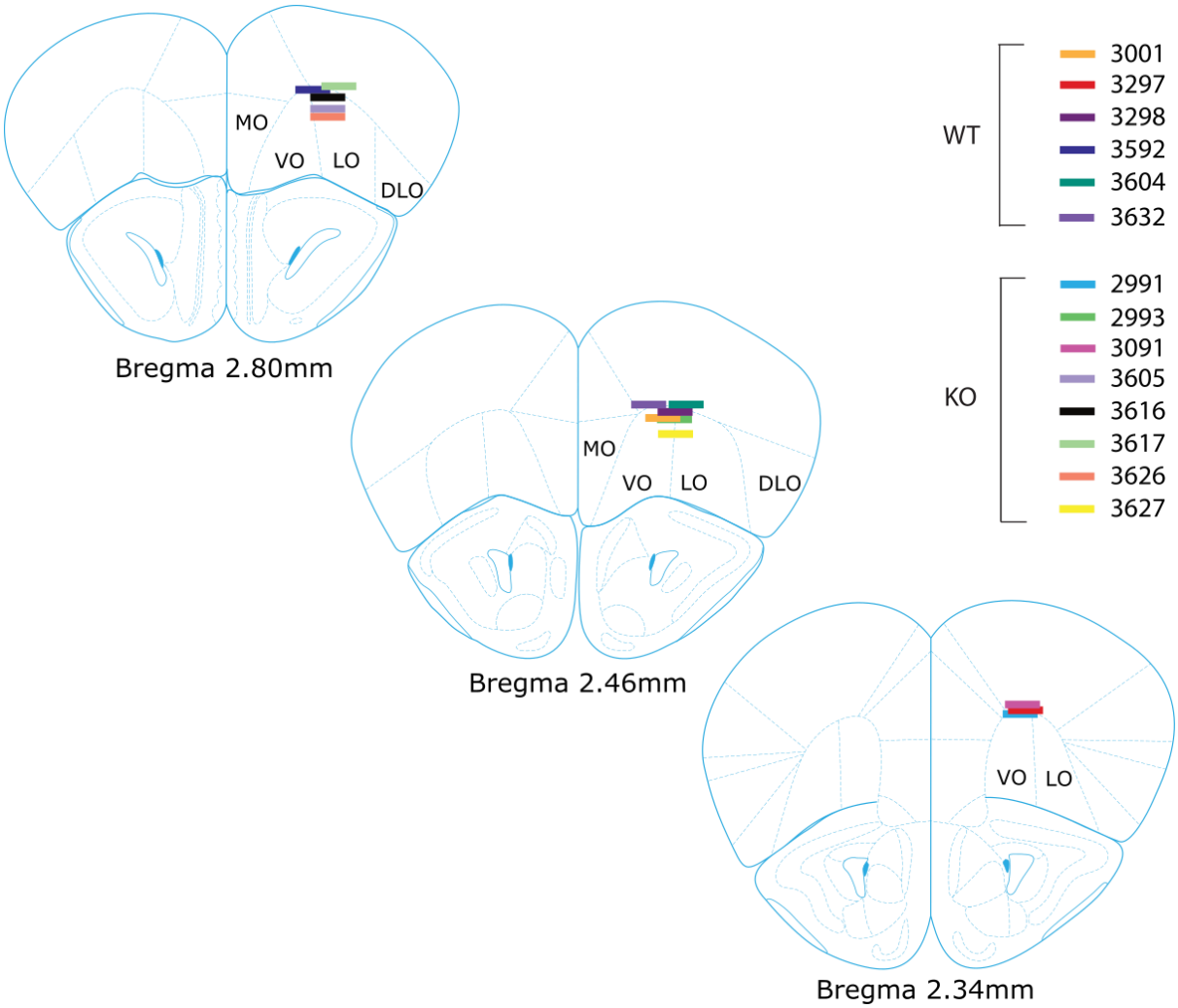

Figure S1: LOFC lens placements across cohort

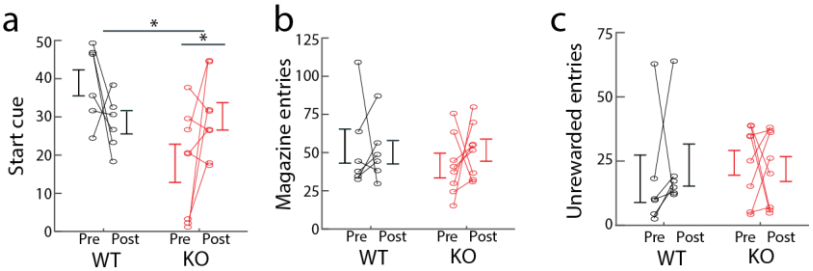

Figure S2: Additional behavioral data from reversal learning task. (a) Start trial cues pre- and post- fluoxetine (genotype: $F_{(1,12)} = 6.9$, $p = 0.02$; drug: $F_{(1,12)} = 0.05$, $p = 0.83$; genotype x drug: $F_{(1,12)} = 6.6$, $p = 0.025$). (b) Total magazine entries (genotype: $F_{(1,12)} = 1.45$, $p = 0.25$; drug: $F_{(1,12)} = 0.25$, $p = 0.62$; genotype x drug: $F_{(1,12)} = 2.31$, $p = 0.15$). (c) Unrewarded magazine entries (genotype: $F_{(1,12)} = 0.29$, $p = 0.6$; drug: $F_{(1,12)} = 0.49$, $p = 0.5$; genotype x drug: $F_{(1,12)} = 1.34$, $p = 0.26$).

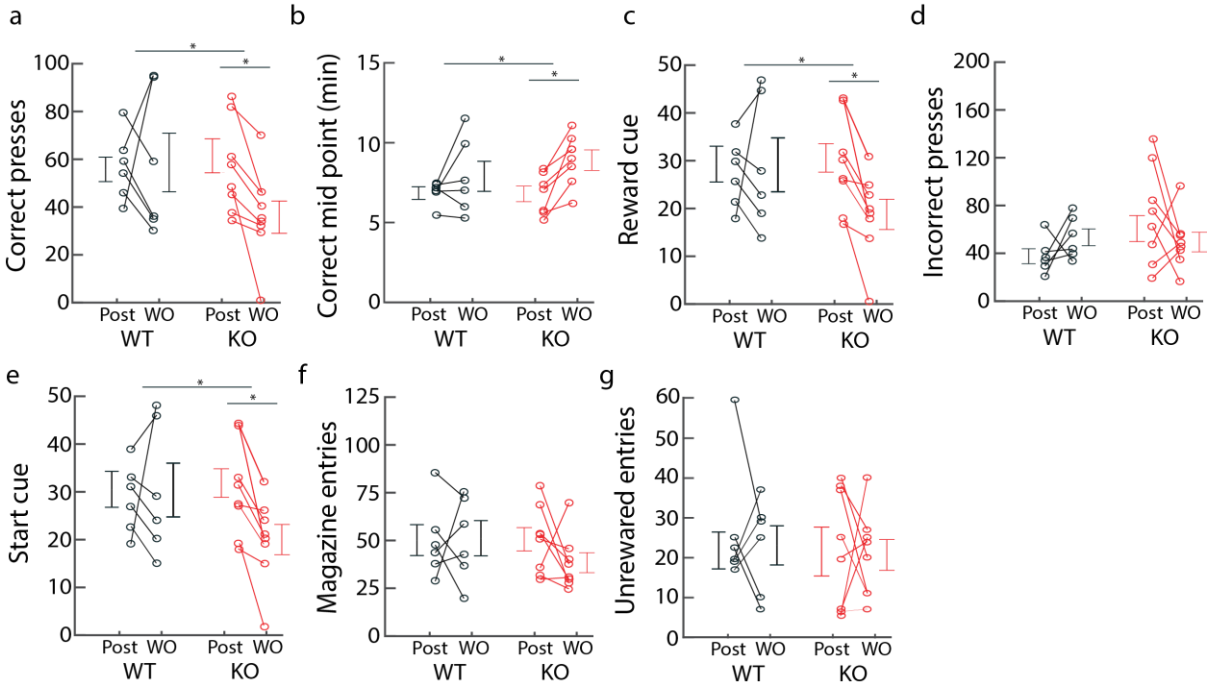

Figure S3: Improvements in reversal learning after fluoxetine treatment disappear after washout (WO). (a) Correct presses (genotype: $F_{(1,12)} = 5.4$, $p = 0.04$; drug: $F_{(1,12)} = 0.76$, $p = 0.4$; genotype x drug: $F_{(1,12)} = 6.78$, $p = 0.02$). (b) Time to acquire correct presses (genotype: $F_{(1,12)} = 4.7$, $p = 0.051$; drug: $F_{(1,12)} = 0.04$, $p = 0.81$; genotype x drug: $F_{(1,12)} = 6.5$, $p = 0.03$). (c) Reward cues (genotype: $F_{(1,12)} = 6.82$, $p = 0.02$; drug: $F_{(1,12)} = 0.04$, $p = 0.83$; genotype x drug: $F_{(1,12)} = 6.61$, $p = 0.02$). (d) Incorrect presses (genotype: $F_{(1,12)} = 0.78$, $p = 0.38$; drug: $F_{(1,12)} = 0.1.3$, $p = 0.26$; genotype x drug: $F_{(1,12)} = 2.31$, $p = 0.15$). (e) Start trial cues (genotype: $F_{(1,12)} = 5.38$, $p = 0.04$; drug: $F_{(1,12)} = 0.48$, $p = 0.51$; genotype x drug: $F_{(1,12)} = 8.0$, $p = 0.01$). (f) Total magazine entries (genotype: $F_{(1,12)} = 1.32$, $p = 0.27$; drug: $F_{(1,12)} = 0.86$, $p = 0.37$; genotype x drug: $F_{(1,12)} = 2.51$, $p = 0.14$). (g) Unrewarded magazine entries (genotype: $F_{(1,12)} = 1.45$, $p = 0.25$; drug: $F_{(1,12)} = 0.21$, $p = 0.65$; genotype x drug: $F_{(1,12)} = 2.29$, $p = 0.16$).

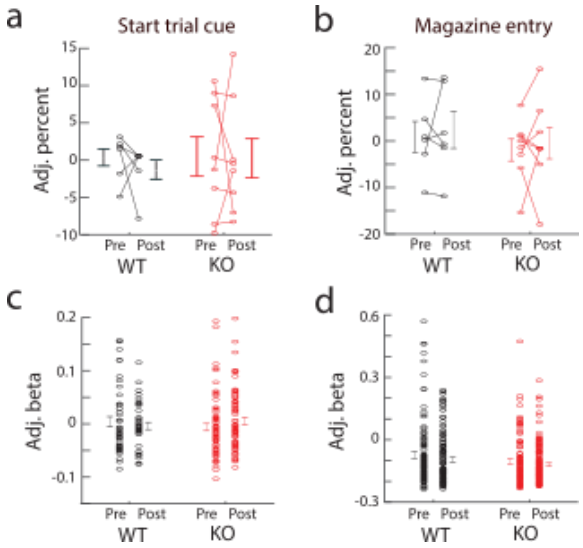

Figure S4: Additional imaging data from the reversal learning task (a-b) Genotype and fluoxetine effects on the percentage of cells encoding (a) trial start cue (genotype: $F_{(1,12)} = 1.48$, $p = 0.24$; drug: $F_{(1,12)} = 0.29$, $p = 0.6$; genotype x drug: $F_{(1,12)} = 1.34$, $p = 0.26$) and (b) magazine entry (genotype: $F_{(1,12)} = 0.49$, $p = 0.49$; drug: $F_{(1,12)} = 0.42$, $p = 0.52$; genotype x drug: $F_{(1,12)} = 1x10^{-5}$, $p = 0.99$). Variables adjusted for number of task events (adj). (c-d) Genotype and fluoxetine effects on the strength of encoding of (c) trial start cue (genotype: $p = 0.34$; drug: $p = 0.54$; genotype x drug: $p = 0.21$) and (d) magazine entry (genotype: $p = 0.65$; drug: $p = 0.29$; genotype x drug: $p = 0.37$. Variables adjusted for number of task events and animal-to-animal variability.

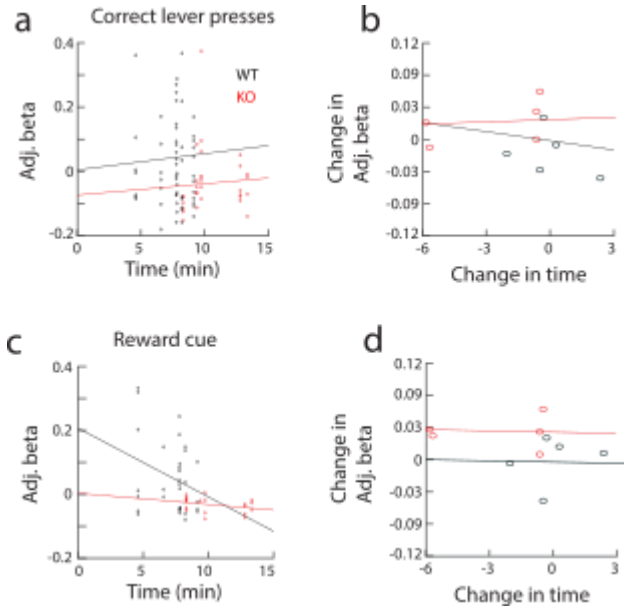

Figure S5: Correlation between strength of encoding and correct midpoint. (a) Adjusted beta weight for correct lever presses vs correct midpoint. (b) Change in adjusted beta weight for correct lever presses pre- and post- fluoxetine vs change in correct midpoint pre- and post- fluoxetine. (c-d) Same as a-b but for strength of encoding of reward cue. All correlations were not significant.

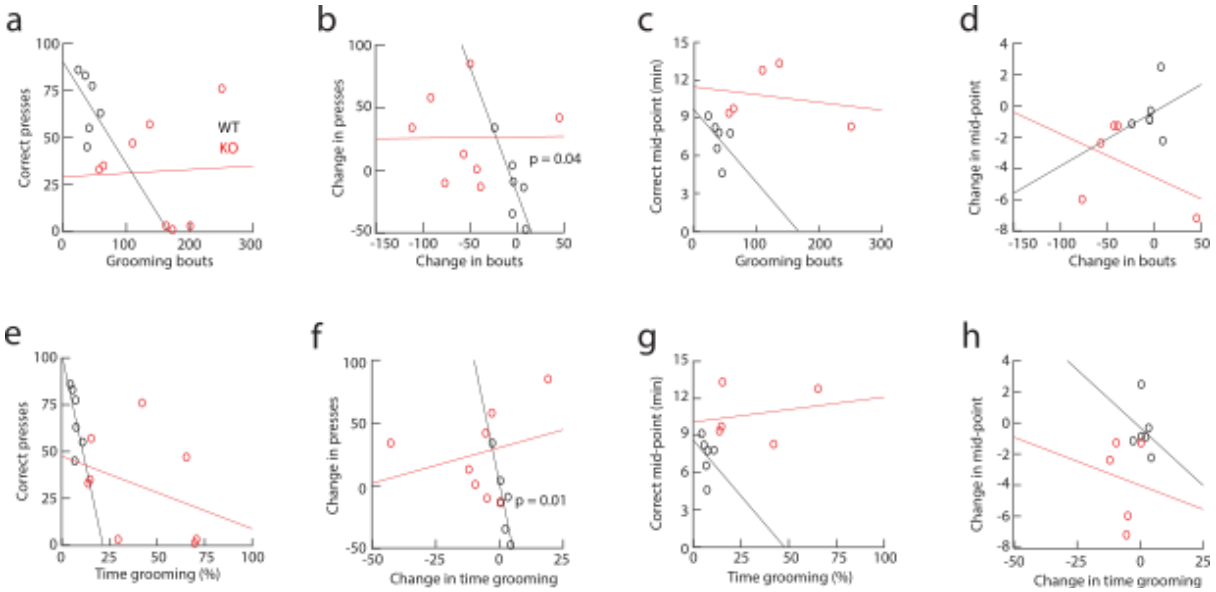

Figure S6: Correlations between grooming and reversal learning behavior. (a) Correct lever presses versus grooming bouts. (b) Change in correct lever presses versus change in grooming bouts. (c) Mid-point of correct lever presses versus grooming bouts. (d) Change in mid-point versus change in grooming bouts. (e) Correct lever presses versus time grooming. (f) Change in correct lever presses versus change in time grooming. (g) Mid-point of correct lever presses versus time grooming. (h) Change in mid-point versus change in time grooming. No correlations were significant unless marked on the graphs.

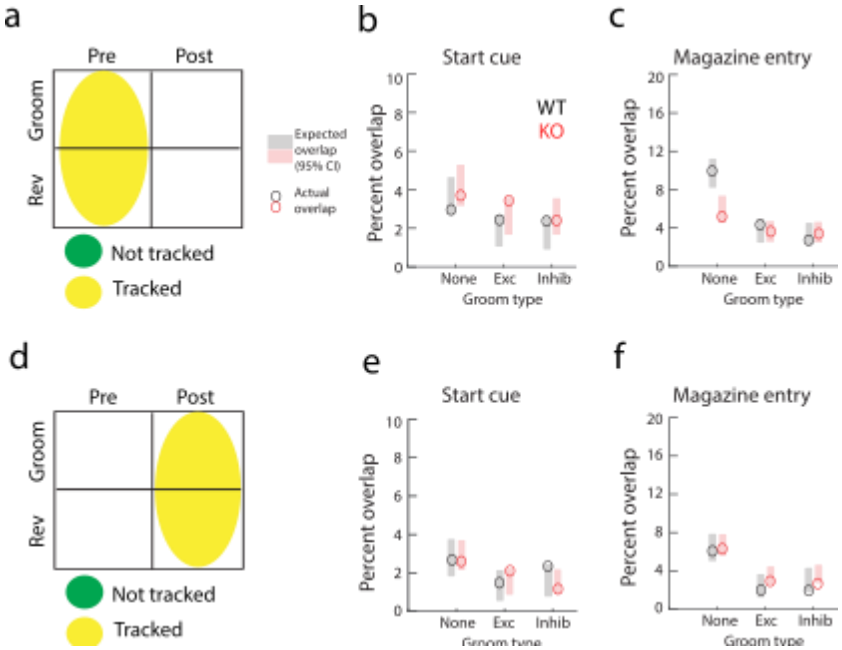

Figure S7: Overlap between additional reversal learning events and grooming. Reversal learning cells are randomly distributed among grooming cells both pre-fluoxetine (a-c) and post-fluoxetine (d-f). Expected overlap (95% CI) between reversal learning and grooming cells (shaded rectangles). Actual overlap between reversal learning and grooming cells (circles). (b) Start trial cue (c) Magazine entries (d-f) Same as a-c but for cells tracked between post-fluoxetine grooming and reversal sessions.

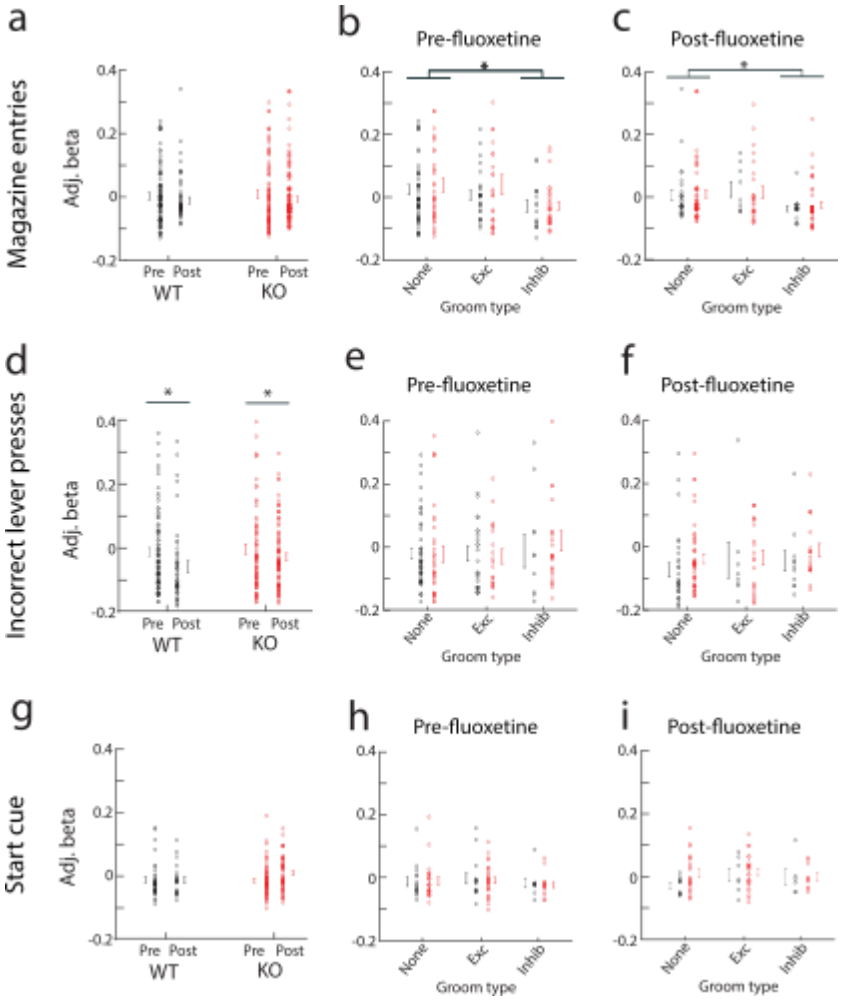

Figure S8: Interaction between additional reversal learning events and grooming. Cells are tracked between grooming and reversal sessions at both the pre- and post- fluoxetine time points. Cells are not tracked between the pre- and post- sessions. (a) Strength of encoding of magazine entries pre- and post- fluoxetine. (b) Strength of encoding of magazine entries pre-fluoxetine grouped by how the cell encodes grooming (genotype: p = 0.48; groom modulation: p = 0.02; genotype x groom mod: p = 0.28; post-hoc t-test groom inhib vs no modulation: p = 0.03). (c) Similar to b but post-fluoxetine treatment (genotype: p = 0.43; groom modulation: p = 0.01; genotype x groom mod: p = 0.61; post-hoc t-test groom inhib vs no modulation: p = 0.01). (d-f) Same as a-c but for incorrect lever presses. (d) Strength of encoding pre- and post- fluoxetine (genotype: p = 0.56; drug: p = 0.02; genotype x drug: p = 0.21). (g-i) Same as a-c but for trial start cue.

Methods supplement

Animals: Sapap3-knockout (*Sapap3*-KO) and wildtype (WT) littermates were generated through breeding *Sapap3* heterozygous mutants (*Sapap3*$^{+/-}$). *Sapap3*-KO (n = 8; 5 female) and wildtype (n = 6; 3 female) littermates were 6-7 months old at the time of first surgery, and imaging experiments were conducted starting at 9-10 months of age, to ensure robust expression of compulsive grooming phenotype in *Sapap3*-KOs.

Calcium imaging surgery: Mice were anesthetized using 5% isoflurane mixed with oxygen and maintained on 1-2% isoflurane for the duration of surgery. Mice were placed on a small-animal stereotactic instrument (Kopf Instruments, Tujunga, CA) and secured using ear bars and a bite bar. Hair was removed from the dorsal surface of the head with hair clippers and the incision area was scrubbed with a betadine solution. A large incision was then made exposing the dorsal portion of the skull. AP and ML measurements were made relative to an interpolated bregma; DV measurements were made relative to dura. 800nl of a virus encoding GCaMP6f under the synapsin promotor (AAV5-synapsin-GCaMP6f-WPRE-SV40, titer $1.82x10^{12}$; Penn Vector Core) was injected into the LOFC adjacent to the lens implant target (AP: +2.7, ML: -1.0, DV: -1.6) using a fixed needle Hamilton syringe (Cole-Parmer Scientific, Vernon Hills IL, USA) connected to sterile polyethylene tubing affixed to a metal cannula and a Harvard Apparatus Pump 11 Elite Syringe Pump (Harvard Apparatus, Holliston MA, USA). Immediately after injection of virus into the LOFC, a 500µm diameter, 6.1mm length gradient refractive index lens (ProView GRIN lens, Inscopix Pala Alto, CA USA) was lowered just dorsal to the viral injection target (AP: +2.6, ML: -1.2, DV: -1.4) to allow for visualization of cells in the target region. GRIN lenses were secured in place with black dental cement (Ortho-Jet, Lang Dental, Wheeling, IL) surrounding the lens and two 0.45mm skull screws were placed just anterior of the lambdoid suture. Following completion of each surgery, mice were injected with sub cutaneous (s.c.) carprofen (3mg/kg in 0.9% saline; Henry Schein, Melville, NY) and administered topical antibiotic ointment (TAO; Henry Schein) and lidocaine HCL 2% ointment (Henry Schein) around the headcap. Mice were then placed on a heating pad and given DietGel (ClearH_2O, Portland ME, USA) and monitored until they were fully recovered from anesthesia. Mice were administered carprofen s.c. and received lidocaine and TAO treatments for 3 days post-surgery. For all surgical procedures mice were kept group housed with same sex littermates.

After ~3-4 weeks for viral incubation, a second procedure was performed during which mice were again anesthetized with isoflurane and secured to a stereotactic apparatus using ear cuffs. Using a Dremel, excess dental cement was carefully removed exposing the ProView GRIN lens. The top of the ProView lens was then cleaned with compressed air, lens paper, and 100% ethanol to remove all dental cement dust. A magnetic microscope baseplate (Part ID:1050-002192, Inscopix) was then attached to the miniaturized microscope (nVistaHD 2.0 epifluorescence microscope, Inscopix) and lowered into place above the GRIN lens with the 475nm blue LED gain and power increased until the lens and gross structures were visible. With isoflurane maintained at 0.5-1%, the optimal field of view was then determined by focusing on visible/active cells or other gross landmarks (blood vessels). Once an optimal field of view was obtained, the baseplate was cemented in place and a plastic Microscope Baseplate Cover (Part ID:1050-002193; Inscopix) was attached to prevent debris from blocking the lens.

Fluoxetine preparation and administration: (±)Fluoxetine hydrochloride (Fluoxetine; NIMH Chemical Synthesis and Drug Supply Program) was administered via drinking water according to established methods (*1, 2*). Briefly, bottles were placed in each cage and drinking was monitored for 3 consecutive days to calculate the concentration necessary to achieve the target 18 mg/kg dose, which produces serum fluoxetine levels comparable to a high dose of fluoxetine that is efficacious in OCD patients (*2*). Based on the average daily consumption and the average weight of the mice in each cage (and in line with historical averages within our lab), 100mg/L fluoxetine hydrochloride was mixed with autoclaved drinking water and stored in black bottles to prevent light degradation. Fluid consumption and bodyweight was continually monitored weekly and bottles

were changed every 4 days to avoid degradation of fluoxetine. After 4.5 weeks of administration, fluoxetine was removed from cages and mice were given a two-week washout from the drug to evaluate whether behavior differences returned to baseline levels.

Experimental timeline:
Experimental design: Mice underwent testing in a repeated measures design, in which all subjects were treated with fluoxetine, and within subject data was compared between baseline, fluoxetine treatment, and drug washout periods. Behavior and neural data were collected weekly for grooming and every other week for reversal learning. On weeks where both behaviors were tested, grooming was tested first, food was removed from the cages that afternoon, and mice underwent operant training for 2 days prior to reversal on the third day (see details below). Grooming was tested at baseline, following 1, 2, 3, and 4 weeks of treatment, and at 1 and 2 weeks during drug washout. Reversal was tested at baseline, 2, and 4 weeks treatment and 2 weeks washout. Data presented here are for baseline and 4 weeks treatment (neural and behavioral data) and washout (reversal behavior data only).
Habituation: Following recovery from baseplate surgery, mice underwent extensive habituation using both the miniature nVista 2.0 microscope, and a “model” microscope that is the same size and weight and can be attached to the animal’s baseplate. Mice were extensively habituated in testing environments used for both grooming and operant training with both model and real microscopes prior to these studies.
Prior testing: Prior to baseline testing, mice underwent >2 weeks operant training (similar to (*3*)) for acquisition of lever pressing (fixed ratio 1 schedule, 1 hour sessions), training on rule 1 (e.g. left lever correct, right lever incorrect; counterbalanced, variable ratio (VR) 2 schedule, 30 minute sessions), first reversal (5 days training rule 2) and second reversal (1 day training rule 1). Thus, mice had extensive experience with operant testing and rule changes prior to baseline testing. Mice were also previously tested in at least 2 x 40 minute imaging sessions for grooming analysis similar to procedures used in these studies.
Grooming imaging procedures: A custom-built behavioral apparatus was constructed for the accurate simultaneous assessment of grooming behavior and neural activity via *in vivo* calcium imaging. A clear plexiglass sheet was suspended over a behavioral acquisition camera (Point Grey Blackfly, FLIR Integrated Imaging Solutions). A clear acrylic chamber (8”x8”x12”) was placed above the camera such that a mouse could be visualized from below. Behavioral acquisition was conducted at 40 Hz using SpinView (Point Grey, Wilsonville, OR) software and detailed frame information was sent directly to a central data acquisition box (LabJack U3-LV, Labjack Corporation, Lakewood CO USA) which was also receiving calcium frame information (20hz) from nVista software. A pseudorandom flashing (30s ITI) LED visible in the behavioral video controlled by custom scripts via an Arduino (Arduino Leonardo, Somerville MA, USA) and sending TTL pulses to the LabJack was used for alignment of behavior and calcium data. Mice were recorded for 40 minutes during grooming analysis sessions.

Following acquisition, behavioral video was converted and compressed (maintaining accurate frame rate information) into .MP4 format using the open source software HandBrake. Videos were then imported into Noldus The Observer XT (Noldus, Leesburg VA, USA) and grooming behavior was manually scored frame by frame. Grooming behavior was scored according to previous reports (*4*) by an observer blind to experimental condition (genotype and drug treatment). A mouse was considered to be grooming if it engaged in any of the following behaviors: 1) Facial grooming: mouse touches its face, whiskers, or head with its forepaws. 2) Body grooming: mouse licks its flank or its ventral surface. 3) Hind leg scratching: mouse uses one of its hind legs to scratch its flank/ear/face. The beginning of a grooming bout was defined as the frame when a mouse made a movement to begin grooming (e.g. a face grooming bout began the frame a mouse lifted its paw off the ground to touch its face). The end of a grooming bout was defined as the frame when a mouse ceased grooming (e.g. a body grooming bout ended when a

mouse moved its snout from its flank). Grooming bouts separated by less than 500ms were collapsed into a single bout; consequently, the minimum amount of time between grooming bouts for all experiments was 500ms.

Operant conditioning imaging procedures: Mice were tested in a reversal learning paradigm using operant chambers containing two retractable levers with cue lights located above the levers. Levers were positioned either side of a reward magazine (Med Associates, Fairfax, VT). For imaging, several modifications were made including: 1) fabrication of custom magazines with Med Associates IR detectors attached which allowed mice to easily access rewards during imaging and allowed detection of head/body entries to the magazine; 2) placement of a textured Perspex floor over the standard bar floor to provide mice with greater stability; 3) extended inner-chamber walls so that the microscope cable could drop straight into the chamber from a hole made in the roof of the sound attenuation chamber, with room for the cable to easily move during exploration of the chamber. MedPC session code included commands to generate outputs corresponding to behavior events (lever press, magazine entry), and these outputs, along with task events of interest (reward delivery, trial start cue) were sent to a central data acquisition box (LabJack) as TTL pulses generated by Med Associates passive connection panel, where they were synchronized in real time with “sync” signals from nVista corresponding to each frame of calcium imaging data acquired.

Mice that had undergone extensive operant training (details in experimental timeline above) were used. For each timepoint mice were tested for three days (30 minutes each). The first two days were tested on the same rule (e.g. left lever correct, right lever incorrect, using the same contingency from their most recent prior test), during which they were trained with the “model” microscope. On the third day the contingency was reversed, and calcium imaging was performed. For all sessions, mice were trained on a VR2 schedule. Upon the start of a trial, both levers were inserted into the chamber and both cue lights above the levers were turned on. When mice completed a rewarded correct response, this resulted in retraction of the two levers, the two cue lights being extinguished, and delivery of a reward pellet (20-mg chocolate-flavored grain-based pellets; BioServ, Flemington, NJ). Reward retrieval (first magazine entry following reward delivery) triggered the start of an inter-trial-interval (ITI) that was randomly set to 5, 6 or 7 seconds duration. If no magazine entry was detected in 10 seconds after reward delivery, the ITI was triggered. At the end of the ITI, a new trial commenced, with the two levers inserted into the chamber and two cue lights turning on. A houselight covered by a red light filter remained lit throughout the session. During studies mice had ad libitum access to food and water, except during operant training when they received restricted food access to maintain 85-90% free feeding body weight. Food was removed on the night prior to operant training, and mice received restricted food access (after operant training) during the 3 day period of operant testing at each timepoint of the study. Neural data and behavior were recorded for 30 minutes but only the first 15 minutes were used for analysis given that all learning had occurred within this time period.

Calcium imaging acquisition, processing and analysis: On imaging acquisition days, the microscope was attached and mice were placed into a temporary holding cage. Mice were given 3-5 minutes after attachment of the microscope for recovery from scruffing and to allow any rapid photobleaching to occur. After this period, mice were carefully placed into the testing arena. nVistaHD software recorded compressed greyscale tiff images at 20 Hz. For all mice, analog gain of the image sensor was set between 1 and 4 while the 470 nm LED power was set between 10 to 30% transmission range. A caliper was used to accurately measure the precise microscope focus such that multiple imaging sessions were conducted with the same field of view. These settings were kept consistent for each mouse throughout all subsequent imaging sessions.

All imaging pre-processing was performed using Mosaic software (version 1.2.0, Inscopix) via custom Matlab (MATHWORKS, Natick MA, USA) scripts. Videos were spatially downsampled by a binning factor of 4 (16x spatial downsample) and temporally downsampled by a binning factor of 2 (down to 10 frames per second). Lateral brain motion was corrected using the registration

engine TurboReg (*5*), which uses a single reference frame to match the XY positions of each frame throughout the video. Motion corrected 10 Hz video of raw calcium activity was then saved as a .TIFF and used for cell segmentation.

Using custom Matlab scripts, the motion corrected TIFF video was then processed using the Constrained Non-negative Matrix Factorization approach (CNMFe), which has been optimized to isolate signals from individual putative neurons from microendoscopic imaging (*6*). Putative neurons were identified and manually sorted by an observer blind to genotype according to previously established criteria (*7*).

Custom Matlab (MATHWORKS) scripts were used to align calcium traces with behavior. Grooming behavior (state events) was exported as timestamps (grooming start and grooming stop) and aligned to Ca^{2+} time by recording 5 consecutive LED pulses (point events). The offset of Noldus behavior time to nVista Ca^{2+} time was then subtracted off leaving the same number of frames for both the behavior and Ca^{2+} fluorescence. Grooming timestamps were then transferred to a binary/continuous trace of the same length and sampling rate (10 Hz) as each Ca^{2+} trace via logical indexing (grooming = 1, not-grooming = 0). For operant data alignment, behavior events and calcium imaging frames were logged on the same timescale (by Labjack) in real time, and custom MATLAB scripts were used to extract behavior time stamps relative to calcium imaging session start time. Timestamps for behavior are converted to the closest matching frame in the calcium recording (maximum error of one frame or ± 100ms at 10 Hz).

Longitudinal tracking of neurons across sessions: Putative neurons identified via CNMFe were matched using a probabilistic modeling method detailed in (*8*). For all analyses, cell matching occurred across two sessions and was performed using the following steps. First, centroid location for all cells were projected onto a single image. Slight rotation and translation difference between sessions were adjusted to achieve maximal cross-correlation between sessions. Probabilistic modeling was then employed to determine which model (centroid distance vs spatial correlation) was optimal for each set of data. For all data, the spatial correlation model yielded the best results and was thus used to match cells across sessions. For final alignment, the spatial correlation (not the joint model) was used, and correlation values for nearest neighbors was set individually for each animal depending on the intersection of the two models.

Encoding model: As described previously (*9*), a multiple linear regression was used to determine how behaviour contributed to neural activity. The dependent variable in the model was the z-scored, denoised calcium traces (F) of putative neurons identified by CMNFe.

For analysis of encoding of grooming, grooming was the only independent variable in the encoding model and was represented as a binary trace with a value of 1 when the animal was grooming and 0 elsewhere. The encoding model for grooming was:

$$F = \beta_0 + \beta_g \omega_g + \varepsilon$$

For analysis of encoding of reversal learning, each of the 5 behavioural events (correct lever presses (c), incorrect lever presses (i), magazine entries (e), reward cues (r), trial start cues (s)) were predictors in the model. Each predictor was represented as a vector of '1's when events occurred and 0 elsewhere. Prior to being included in the model, each predictor was convolved with a 3s Gaussian.

$$F = \beta_0 + \beta_c \omega_c + \beta_i \omega_i + \beta_e \omega_e + \beta_r \omega_r + \beta_s \omega_s + \varepsilon$$

For both encoding models, F is the calcium trace, ω is the behaviour predictor, β is the regression coefficient, and ε is a Gaussian noise term. The β values were calculated using the least squares criterion.

To determine whether individual behaviours were significantly encoded in each neuron, we ran two models: a full model containing all behavioural variables, and a partial model excluding the variable of interest. We then calculated an F-statistic for a nested model comparison between the partial model and the full model. We then created a null distribution of the same F-statistic. To do this we created 1000 instances of a shuffled calcium trace by shuffling non-overlapping 3s bins to preserve the autocorrelation of the calcium trace. If the true F-statistic was greater than 3 standard

deviations than the mean of the null distribution then the neuron significantly encoded the behaviour.

If a neuron significantly encoded the behaviour, the strength of encoding was quantified using the regression coefficient (β).

Statistical analysis: Effects of genotype and fluoxetine on behavior were assessed using repeated measures ANOVA, except for bout length analysis which used Kolmogorov-Smirnov test to compare cumulative distribution frequencies between groups. For both grooming and reversal learning imaging analyses, effects of genotype and fluoxetine on percentages of cells modulated and strength of encoding were assessed using repeated measures ANOVA and linear regression, respectively. Percentages of cells modulated by reversal learning were adjusted for differences in the number of behavioral events. Beta weights of cells modulated by reversal learning were adjusted for animal-to-animal variability and number of behavioral events. Percentage of cells and beta weights for grooming analyses were not adjusted for the number of grooming events because all KOs had a higher number of grooming bouts compared to than WTs. Consequently, it was impossible to dissociate genotype effects from the effects of the number of grooming bouts.

Analysis of expected versus actual overlap between grooming and reversal learning: Data were pooled across all animals within genotype. To determine whether the actual overlap between reversal learning and grooming-encoding cells was different from that which would be expected by chance, we performed a bootstrap analysis. For each of the 5 behaviors examined for reversal learning, we found the total number of neurons that encode that behaviour. As an example, for each genotype we calculated the total number of neurons encoding the correct lever press ($N_{correct}$) and the total number of neurons inhibited by grooming (N_{groom_inh}). The actual overlap in the population is the percentage of neurons that encode both the correct lever press and are inhibited by grooming. To construct the expected overlap, we randomly chose a sample of neurons (N_{random}) equal to $N_{correct}$ and calculated the percent overlap between N_{random} and N_{groom_inh}. We repeated this procedure 1000 times to construct a distribution of the expected overlap between grooming and reversal learning populations. The 95% confidence interval of this distribution was represented as the shaded rectangles in Fig. 6,S7. We consider the populations to be overlapping, segregated or randomly overlapping if the actual overlap is greater, less than or within the 95% CI of the expected overlap, respectively.

Supplement References

1. S. E. Ahmari *et al.*, Repeated cortico-striatal stimulation generates persistent OCD-like behavior. *Science* **340**, 1234-1239 (2013).
2. S. C. Dulawa, K. A. Holick, B. Gundersen, R. Hen, Effects of chronic fluoxetine in animal models of anxiety and depression. *Neuropsychopharmacology : official publication of the American College of Neuropsychopharmacology* **29**, 1321-1330 (2004).
3. E. E. Manning, A. Y. Dombrovski, M. M. Torregrossa, S. E. Ahmari, Impaired instrumental reversal learning is associated with increased medial prefrontal cortex activity in Sapap3 knockout mouse model of compulsive behavior. *Neuropsychopharmacology : official publication of the American College of Neuropsychopharmacology* **44**, 1494-1504 (2019).
4. A. V. Kalueff *et al.*, Neurobiology of rodent self-grooming and its value for translational neuroscience. *Nature reviews. Neuroscience* **17**, 45-59 (2016).
5. K. K. Ghosh *et al.*, Miniaturized integration of a fluorescence microscope. *Nature methods* **8**, 871-878 (2011).
6. P. Zhou *et al.*, Efficient and accurate extraction of in vivo calcium signals from microendoscopic video data. *Elife* **7**, (2018).
7. S. L. Resendez *et al.*, Visualization of cortical, subcortical and deep brain neural circuit dynamics during naturalistic mammalian behavior with head-mounted microscopes and chronically implanted lenses. *Nature protocols* **11**, 566-597 (2016).
8. L. Sheintuch *et al.*, Tracking the Same Neurons across Multiple Days in Ca(2+) Imaging Data. *Cell Rep* **21**, 1102-1115 (2017).
9. B. Engelhard *et al.*, Specialized coding of sensory, motor and cognitive variables in VTA dopamine neurons. *Nature* **570**, 509-513 (2019).